MoO_3 altered ZnO: A suitable choice for the photocatalytic removal of chloro-acetic acids in natural sunlight exposure

M. Tariq Qamar, M. Aslam, Z.A. Rehan, M. Tahir Soomro, Ikram Ahmad, Muhammad Ishaq, Iqbal M.I. Ismail, P. Fornasiero, A. Hameed

PII: S1385-8947(17)31315-3
DOI: http://dx.doi.org/10.1016/j.cej.2017.07.168
Reference: CEJ 17434

To appear in: *Chemical Engineering Journal*

Received Date: 5 May 2017
Revised Date: 20 July 2017
Accepted Date: 28 July 2017

Please cite this article as: M.T. Qamar, M. Aslam, Z.A. Rehan, M.T. Soomro, I. Ahmad, M. Ishaq, I.M.I. Ismail, P. Fornasiero, A. Hameed, MoO_3 altered ZnO: A suitable choice for the photocatalytic removal of chloro-acetic acids in natural sunlight exposure, *Chemical Engineering Journal* (2017), doi: http://dx.doi.org/10.1016/j.cej.2017.07.168

MoO_3 altered ZnO: A suitable choice for the photocatalytic removal of chloro-acetic acids in natural sunlight exposure

M. Tariq Qamar[1,2], M. Aslam[1], Z. A. Rehan[3], M. Tahir Soomro[1], Ikram Ahmad[2], Muhammad Ishaq[4], Iqbal M. I. Ismail[1,2], P. Fornasiero[5], A. Hameed[1,6*]

[1]Centre of Excellence in Environmental Studies (CEES), King Abdulaziz University, Jeddah- 21589, Saudi Arabia.

[2]Chemistry Department, Faculty of Science, King Abdulaziz University, Jeddah- 21589, Saudi Arabia.

[3] Department of Polymer Engineering, National Textile University, Faisalabad-37610, Pakistan

[4]Department of Chemistry, Quaid-i-Azam University, Islamabad- 45320, Pakistan.

[5]Department of Chemical and Pharmaceutical Sciences, ICCOM-CNR, University of Trieste, 34127 Trieste, Italy

[6]National Centre for Physics, Quaid-i-Azam University, Islamabad- 44000, Pakistan

ABSTRACT

The MoO_3 coated ZnO photocatalysts were synthesized for the optimum harvesting of the absorbed ultraviolet sunlight photons by initially permeating Mo^{6+} ions at the surface of pre-synthesized ZnO and finally transformed to MoO_3 by thermal treatment in the air. The absorption spectra of the synthesized powders revealed the extension of the absorption edge in the visible region whereas, the photoluminescence spectroscopy established the supporting role of the MoO_3 coating in gradually plummeting the excitons recombination. The growth of additional peaks in Raman as well as x-ray photoelectron spectra and the appearance of the

corresponding low-intensity reflection substantiated the surface prevalence of MoO_3. The absence of the individual particles of MoO_3 in FESEM and the verification of coated layer by HRTEM images validated the authenticity of the adopted synthetic route. The electrochemical evaluation of the synthesized powders under illumination revealed the complete elimination of photocorrosion and the synergic role of the MoO_3 layer for improved trap and transfer of charge carriers. The evaluation of the flat-band potentials of the coated powders by Mott-Schottky analysis revealed the suitability of the conduction band edges for the generation of superoxide anion radicals. The photocatalytic activity of the synthesized powders was assessed for the removal of chloro derivatives (mono-, di-, trichloroacetic acids) in comparison to pure acetic acid. A significant effect of the stability, polarity and stereochemical structure of the substrate on the photocatalytic removal process was observed and discussed. The experimental evidences from the time-scale chemical analysis were interpreted for the identification of the reactive oxygen species (ROS) involved in the degradation/mineralization process. The validation of the Langmuir-Hinshelwood kinetic model was also examined. Efforts were made to estimate the plausible route of the degradation/mineralization process.

Keywords: Sunlight photocatalysis, MoO_3 coated ZnO, Acetic acid, Chloroacetic acids

1. Introduction

The growing world demand for "clean water" necessitates the development of a cost-effective, efficient and user-friendly tool for the decontamination of wastewater. It is generally accepted that the advanced oxidation processes (AOP) based on photocatalytic technologies are the most sustainable approach to solve this problem [1,2]. However, this demands the exploration of sunlight responsive efficient photocatalysts with the choice to discover either the new semiconductor combinations or to alter the existing active catalysts [3-6]. In this context, TiO_2 has been a subject of the large majority of investigations with appreciable improvements in

light harvesting and photoactivity [7]. Nevertheless, there is still a huge need of amelioration of existing materials, to enhance light absorption, especially in the visible portion of the solar spectrum, to improve material stability, to reduce photo-generated charge carrier recombination phenomena [8-12]. From this approach, many new materials have been proposed and investigated as an alternative to the benchmark TiO_2 and its doped, nanostructured or hybridized forms [13]. Among the other explored metal oxide semiconductors, ZnO, because of its physical and optical properties, has partially attracted the attention of the scientific community as a suitable replacement to TiO_2, however, often been ignored because of its low resistance towards excitons recombination (radiative emission) and instability under illumination [14-16]. ZnO is a highly fluorescent material, but amazingly has comparable photocatalytic activity with TiO_2 that suggest the possibility of further improvement in the activity and stability under illumination by smearing apposite surface alteration [17-19]. Several strategies of surface modifications that include composite formation, metal impregnation and doping of semiconductors are reported in the literature [20, 21]. However, the approach of coating the surface by metal impregnation established to be an auspicious method because it is easy, convenient and effective, both for avoiding recombination and enhancing the stability of ZnO [20, 22, 23].

Among the prominent organic pollutants, the derivatives of chloroacetic acid (CAA) such as mono-, di- and tri-chloroacetic acid, due to polarity, hydrophilic and highly phytotoxic nature are the contaminants of interest. These toxicants not only originated from volatile precursors, but also produced as by-products during the biological decontamination (chlorination) of water [24-29]. At our knowledge the detailed investigations on the photocatalytic removal of these derivatives are rare in the literature [30-32].

The current study is an effort in this direction and aims to develop photocorrosion resistant sunlight active photocatalyst for water decontamination by coating the surface of ZnO with different wt% loadings of MoO_3. The optical and structural characterization of synthesized materials was performed by DRS, PL, XRD, XPS and Raman spectroscopy respectively. The morphology and homogeneity of materials were examined by FESEM and HRTEM. The staircase potential electrochemical impedance spectroscopy (SPEIS) was employed to evaluate the flat-band potential and band edge potentials whereas the stability of the coated materials under illumination were assessed by cyclic voltammetry (CV). The charge transport and retention ability of the MoO_3 coating were investigated by electrochemical impedance

spectroscopy (EIS) and chronopotentiometry (CP). The photocatalytic activity of the MoO_3 modified ZnO was evaluated for the degradation of mono-, di- and trichloro derivatives of acetic acid under natural sunlight (daylight) irradiation. Contrary to traditional analytical tools, the simultaneous variations in the concentration of respective ions, during the degradation process, was monitored by ion chromatography (IC). The potential of mineralization of the coated catalysts was assessed by total organic carbon (TOC) measurements. The reusability of the catalyst with optimum activity was also investigated. Finally, the results from the various analytical tools were correlated to propose the plausible route of degradation/mineralization.

2. EXPERIMENTAL

2.1. Synthesis of MoO_3 coated ZnO

MoO_3 coated ZnO photocatalysts were synthesized by impregnating Mo^{6+} ions on pre-synthesized ZnO. The synthesis of hexagonal ZnO was carried out by the slow hydrolysis of zinc acetate using 0.1 M KOH [33]. The wet impregnation method [34] was used for the synthesis of 0.5, 1, 3, and 5 wt% of MoO_3 coated ZnO catalysts. In a typical synthesis of 0.5wt% Mo^{6+} deposited ZnO, 0.092g of $(NH_4)_6Mo_7O_{24}\cdot 4H_2O$ (Sigma-Aldrich, 99.99%), containing 0.5 wt% Mo^{6+} ions with respect to the weight of ZnO, was dissolved in 50 ml of deionized water followed by the addition of Triton X-100 as a surfactant under stirring. The precisely weighed amount of ZnO (10 g) was added to the Mo^{6+} solution. The slurry was aged overnight till dryness at 100^{o}C under constant stirring for maximum deposition of Mo^{6+} ions at the surface of ZnO. For complete conversion of impregnated Mo^{6+} ions to MoO_3, the dried powder was calcined at 500°C for 4 h in a muffle furnace with the heating and cooling rate of 10^{o}C/min. The other compositions were synthesized accordingly and identified as 0.5, 1, 3 and 5 wt% MoO_3 coated ZnO.

2.2. Characterization of coated photocatalysts

The solid-state absorption and diffuse reflectance spectra (DRS) of the synthesized MoO_3 coated ZnO photocatalysts were acquired by UV-visible diffuse reflectance spectrophotometer (Lambda 650, Perkin Elmer, USA) in the 190-900 nm range. The %R data were subjected to Kubelka-Munk transformation, F(R), for the evaluation of direct absorption edges by plotting $(F(R) \times h\upsilon)^2$ versus $h\upsilon$ (eV). The photoluminescence (PL) emission spectra of the synthesized powders were recorded by a fluorescence spectro-fluorophotometer (RF-5301 PC, Shimadzu,

Japan) at an excitation wavelength of 200 nm while the fluorescence emissions were recorded in the range of 300 to 800 nm. A DXR Raman Microscope (Thermo Scientific, USA,) equipped with 532 nm laser as the excitation source at 6mW power measured the Raman shifts. The powder XRD patterns of bare and MoO_3 coated ZnO powders were recorded by X'Pert X-ray powder diffractometer (PW1398, Philips, Netherlands) equipped with Cu *Kα* radiation source, in the 2θ range of 20° to 90° with a step time of 3 seconds and step size of 0.05^{o}. Scherer's equation was applied on intense reflections to evaluate the crystallite size of various phases. The variations in the oxidation states of Mo and Zn were estimated by x-ray photoelectron spectroscopy (XPS) in the binding energy range of 0 eV to 1350 eV by X-ray Photoelectron Spectrometer (PHI 5000 Versa Probe II, ULVAC-PHI Inc., USA). The morphology of the synthesized powders was examined by Field Emission Scanning Electron Microscope (FEI, Quanta FEG 450, Quorum Q150R ES, Quorum Technologies Ltd., England) at a voltage of 30kV. Prior to imaging, the samples were coated with gold. The fine structural analysis was performed by transmission electron microscopy (TEM), (JEM2100F, JEOL, Japan) operated at 200KV. For the analysis, a 2-3 mg sample powder was dispersed in 10 ml of methanol by sonication. A 5 µL drop of dispersed sample was dried on 3mm carbon-coated Cu grid and degassed for 30 min at 50 $^{\circ}$C in a vacuum desiccator.

2.3. Photoelectrochemical investigations

The Mott-Schottky analysis was performed by sweeping the potential in the range of -1.5 to +1.5 V versus saturated calomel electrode (SCE) with an AC frequency of 1 kHz and an amplitude of 10 mV, both in the dark and under illumination. The working electrodes were prepared by casting off 10 µl of the 2:1 (2 mg photocatalyst in 1 mL of 0.1% Nafion solution) suspension onto a glassy carbon electrode. The ability of MoO_3 coated layers in suppressing the photocorrosion, compared to pure ZnO, under illumination, was evaluated by cyclic voltammetry (CV) using a VSP multi-channel potentiostat (Bio-logic Science Instrument, USA) equipped with Ec-lab software in a three electrode system, namely; glassy carbon electrode (working electrode), platinum (counter electrode) and Ag/AgCl saturated electrode (reference electrode). The powders, dispersed in chloroform, were coated at the tip of glassy carbon electrode by dropping 10µl of suspension and dried in hot air for film formation. The homogeneity of the film was analyzed optically. For acquiring cyclic voltammograms under illumination, a 50-watt

halogen lamp was used as a light source. The cyclic voltammograms acquired for the coated samples, both in the dark and under illumination, were compared with that of pure ZnO. All the measurements were carried out at room temperature (25^{o}C).

2.4. Evaluation of Photocatalytic activity

The photocatalytic activity of pure and MoO_3 coated ZnO powders in sunlight exposure was evaluated by exposing 150 ml of respective acetic acid and haloacetic acid solutions (50 ppm each) containing the optimized amount (150 mg) of respective catalyst in a Pyrex® glass reactor. The dimensions of the glass reactor were 15.5 (diameter) × 2.5 (height). The evaluated effective surface area of the reactor was 189 cm^2. The photocatalytic experiments were performed under sunlight illumination of $800\pm100\times10^2$ lx (21.4939^{o} N, 39.2503^{o} E) in the month of December-January for a fixed period of the daylight i.e. from 9:30 am to 3:00 pm without stirring. Prior to exposure, the adsorption-desorption equilibrium between the catalysts and substrates was established by stirring the samples in the dark for 30 min. The optimization of the MoO_3 coating was performed by using MCAA as substrate. The amount of the catalysts was optimized for pure ZnO and kept constant for rational comparison. The progress of degradation process was monitored by drawing the samples after every 20 mins in the first hour, after 30 min in the second hour and after 60 min in the last two hours. The catalyst was removed by using 0.20µm Whatman syringe filter. The collected samples were analyzed by ion chromatography, Dionex (ICS-5000 + EG Eluent Generator), Thermo scientific, USA, to measure the released ions during a photocatalytic process. The progress of the removal process was monitored by ion chromatography (IC) in two different operational modes. The isocratic approach was employed to measure the instantaneous decrease and simultaneous increase in the in the concentration of substrates and released chloride ions, respectively, whereas the complete profiling of all the released anions was accomplished by gradient mode. TOC-VCPH total carbon analyzer supplied by Shimadzu Corporation, Japan, measured the total organic carbon (TOC) of the samples. Blank experiments were performed to estimate the decrease in concentration of the substrates by direct photolysis.

3. RESULTS AND DISCUSSION

3.1. Characterization of Photocatalysts

The comparison of the reflectance spectra of the ZnO, MoO_3, and MoO_3 altered ZnO is presented in Fig. 1a. A mild decrease in the %R with the increasing coating level is noticeable. The appreciable decrease for 1 wt% MoO_3 coated sample in 400 to 900 nm suggests an optimal thickness of the coated layer. The solid-state absorption spectra, as shown in Fig. 1b, directly indicate the beneficial role of the presence of MoO_3 in enhancing visible light absorption, with the maximum effect for 1 wt% MoO_3 coated sample. The observation highlights the important role of Mo^{6+} based phases on extending the spectral response in the visible region. The coated MoO_3 introduced additional Mo^{6+} ($4d^0$ $5s^0$) orbitals in the vicinity of the conduction band (Zn $3d^{10}4s^0$) of ZnO. The direct transitions from the valence band (O 2p) to the newly defined-low laying conduction band by the Mo^{6+} entities resulted in the shifting of the absorption edge to the visible region. The bandgap values, calculated by means of Kubelka-Munk transformation (Fig. 1 c and d) for pure MoO_3, ZnO and coated samples (0.5, 1, 3 and 5wt% MoO_3) were ~2.87, ~3.1, ~2.9, ~2.85, ~2.94, and ~2.95 eV, respectively. The observed values for the MoO_3 and ZnO were in close agreement with the literature values [35]. The 0.5 and 1wt% MoO_3 coated ZnO samples exhibited a mild lowering in the bandgap energy as compared to bare ZnO whereas for 3 and 5wt% MoO_3 coated samples, the major contribution appeared from the MoO_3 coating because of the optimal surface coverage.

The comparison of the PL spectra of pure MoO_3 and ZnO with those of the MoO_3 coated powders is presented in Fig. 1e. For the pure ZnO and MoO_3, the bands centered at ~402.3 nm and ~448.3 nm specified the bandgap de-excitations. The calculated bandgap energies of ~3.08 eV and ~2.77 eV were in accordance with the DRS analysis. The broad band with the sharp maxima at ~464 nm in the emission spectra of ZnO represented the de-excitations of the electrons trapped in the defect states, whereas the broadening of the band furnishes the rough estimate of the density of the trapping sites at the surface of the material. Variations in the morphology account for the minor variations in the positions of these bands with respect to the literature [33]. Additionally, the intensity of the emission for ZnO was significantly higher than that of MoO_3. A significant decrease in the intensity of both the bands was noticed even with the minimum coating level of 0.5 wt%. A successive decrease in the intensity with the increasing surface density of MoO_3 signified the supporting role of the coated layers in suppressing the exciton recombination process. A decrease of ~16, ~23, ~42 and ~53% in the intensity of the

band at ~402.3 nm was observed for 0.5, 1, 3, and 5 wt% MoO_3 coated ZnO powders, respectively.

The major Raman active bands of pure ZnO were observed at ~334.84, ~388.39, ~438.50, ~535.40 and ~1154.92 cm^{-1} [33]. The comparison of the Raman spectra of bare and MoO_3 coated ZnO (Fig. 1f) evidences a significant decrease in the intensity of the E_2 band of ZnO at 438.50 cm^{-1} originated by the vibrations of surface Zn^{2+}-O^- groups and the appearance of the additional bands, in 900 to 1100 cm^{-1} region, with the increasing MoO_3 coating. The substantially decreased intensity of the E_2 band even at the lower MoO_3 coating, i.e. 0.5 and 1 wt%, indicates a strong interaction between surface oxygen and Mo^{6+}. The intensity decrease becomes more significant as the surface coverage increases. For 3 wt% MoO_3 coated ZnO, the appearance of the additional doublet at ~947.69 and ~966.97 cm^{-1} can be attributed to the stretching of Mo=O and MoO^-, respectively. An enhanced intensity of the doublet was noticed with the further increase in the MoO_3 coating with the appearance of additional bands in 800 to 900 cm^{-1} verified the bending and asymmetric stretching of Mo-O-Mo bonds.

The XRD patterns of the pure MoO_3, ZnO, and MoO_3 coated ZnO are presented in Fig. 2a. The major reflections due to pure ZnO at the 2θ values of 31.73° (51%), 34.39° (38.6%), 36.20° (100%), 47.50° (28.3%), 56.55° (48.7%), 62.80° (45.7%) and 67.9° (40.6%) were in accordance with that of hexagonal ZnO (JCPDS 36-1451) [23, 36] whereas that of MoO_3 matched with monoclinic phase (JCPDS 47-1081). In the coated samples, apart from the variations in the intensity of the reflections, probably, the intense reflections of ZnO over shadowed the reflections due to the low (0.5 and 1wt%) MoO_3 coatings. However, a mild growth of the additional XRD reflections was noticed in 3 and 5wt% MoO_3 coated samples. The exploded view of the XRD patterns showing the progress of additional reflections in the 2θ range of 20 to 30º is presented in Fig. 2b. The XRD analysis revealed the presence of monoclinic MoO_3 (JCPDS 47-1081) as the major phase, whereas low-intensity reflections also indicated the existence of triclinic $ZnMoO_4$ (JCPDS 35-0765). It might be anticipated that the interaction of the Mo^{6+} with the surface oxygen shared by Zn^{2+} results in the formation of surface $ZnMoO_4$ whereas the successive layer deposit as MoO_3. In the evaluation of the average crystallite sizes of the coated powders, in comparison to pure ZnO, a mild increase till 3wt% MoO_3 coating followed by a decrease for 5wt% was witnessed. The evaluated average crystallite sizes of bare,

0.5, 1, 3 and 5wt% MoO_3 coated ZnO powders were ~50.70, ~53.22, ~54.50, ~55.80, and ~48.3 nm, respectively.

The comparison of the typical wide angle XPS survey scans of 3 wt% MoO_3 coated ZnO powder before and after the surface etching is presented in Fig. 3, where the peaks due to O1s, Zn2p, and Mo3d core level are observable. The binding energy value of 284.6 eV for C1s (internal standard) was used to correct both the spectra. As presented in the inset (a) and (b) of Fig. 3, apart from the minor variations in the peak symmetries and intensity, the etching resulted in no significant disparities in the binding energies. The precise binding energies of the spin-orbit splitted Mo3d, O1s and Zn2p core levels, before and after etching, were recognized by the narrow-angle scanning and Gaussian fitting of each component. The fitted spin-orbit split Mo3d ($Mo3d_{5/2}$ and $Mo3d_{3/2}$) core levels before and after the etching is presented in Fig. 4a and b respectively. The mild asymmetry of the original high precision doublet of Mo3d, before etching, revealed the existence of additional oxidation states or Mo^{6+} in the dissimilar chemical environment. The deconvolution of the splitted peaks ($Mo3d_{5/2}$ and $Mo3d_{3/2}$) disclosed the major set of peaks at ~232.79 and ~235.9 eV representing the $3d_{5/2}$ and $3d_{3/2}$ levels respectively of Mo^{6+} of coated MoO_3. In addition to the major Mo^{6+} peaks, two additional sets of low-intensity peaks at lower and higher binding energies as compared to that of principle Mo^{6+} peaks were also observable. The set of minor peaks of lower binding energy values of ~232.2 and ~235.38 eV represented the $3d_{5/2}$ and $3d_{3/2}$ levels of Mo in the 5+ oxidation state. The identification of Mo^{5+} states indicated the existence of minor oxygen defects in the coated layer as a consequence of the adopted synthetic route. The set of minor peaks at higher binding energy values of ~233.55 and ~236.66 eV for $3d_{5/2}$ and $3d_{3/2}$ splitted levels also corresponded to Mo^{6+} however, originated from the surface $ZnMoO_4$ in the interfacial region. After etching, although, a mild red shift in the binding energies of the deconvoluted components was noticed, however, the binding energy difference of ~3 eV between the splitted $Mo3d_{5/2}$ (~232.5 eV) and $Mo3d_{3/2}$ (~235.5 eV) remained unaffected before and after the etching. The enhanced intensities of the peaks at ~231.83 ($Mo3d_{5/2}$) and ~235.04 eV ($Mo3d_{3/2}$) revealed the escalated generation of Mo^{5+} states under etching. As presented in Fig. 4c and d, the etching revealed no significant change in the symmetry of the O1s peak. The deconvolution of the O1s peaks, before and after the etching, exposed four submerged states at distinct binding energies of ~530.1, ~531.09, ~531.77 and ~532.50 eV before etching and that of ~529.95, ~530.74, ~531.52 and ~532.51 eV after etching.

The variation in the binding energy values disclosed their origin from the chemically different environment. After etching, the most intense peak at ~529.95 eV, assigned to the oxygen attached directly to Zn^{2+} species (Zn^{2+}-O), was in accordance with that reported for ZnO [33]. The peak at ~530.74 eV corresponded to Mo^{6+}-O bonds of the coated MoO_3 layer, whereas the peaks at ~531.52 eV and ~532.51 eV represented the $ZnMoO_4$ and surface hydroxyl groups of adsorbed H_2O respectively. The $Zn2p_{3/2}$ peaks, before and after the etching, are compared in Fig. 4e and f. As per initial observation, although the near symmetric peaks revealed no major change in the chemical environment of Zn^{2+} however, the deconvolution indicated the fraction of Zn^{2+} entities originating from the different chemical environment other than ZnO. The intense $Zn2p_{3/2}$ peaks in the binding energy (BE) values of ~1021.88 eV and ~1021.57 eV respectively, were assigned to the Zn^{2+} of ZnO base and were in accordance with the literature values [33]. The low-intensity $Zn2p_{3/2}$ peaks at ~1022.91 and ~1022.81 eV respectively specified the Zn^{2+} attached to $ZnMoO_4$ in the interfacial region. The minor discrepancy in the observed and literature values is probably due to the matrix effect and the adopted experimental conditions [37].

The high-resolution FESEM images of pure ZnO, 1, 3 and 5wt% MoO_3 coated ZnO catalysts, are compared in Fig. 5a-d. A wide particle size distribution of hexagonal ZnO particles is observable in the image of pure ZnO (Fig. 5a). The fraction of the particles having the particle size $\geq$ 100 nm was significantly lower. The majority of the particles ranged between 10 to 80 nm in size. No significant change in the morphology of the ZnO particles depicted the homogeneous distribution of the MoO_3 all over the surface without the formation of individual particles. Additionally, the aggregation of the ZnO particles with the increasing MoO_3 coating was also not observed. The gradual diminution of the sharp margins of the hexagonal particles with the increasing surface density of MoO_3 indicated the deposited layer at the surface.

The uniform coating of the ZnO particles was further authenticated by TEM analysis. The typical TEM images for 5wt% MoO_3 coated ZnO, at various resolutions, focusing the particles of various sizes are presented in Fig. 6a and b where the ZnO particles entrapped in the coated layers of MoO_3 are noticeable. Additionally, no noticeable effect of the MoO_3 coated layer on the morphology of ZnO was observable whereas the uniformity of the coating was independent of the size of ZnO particles. The HRTEM image focusing the interfacial region is presented in Fig. 6c, where two discrete lattice fringes corresponding to the coated MoO_3 layer and the ZnO

base material are evident. The measurement of the interlayer spacing of the individual lattice planes is presented in Fig. 6d. The measured d-spacing of 0.268 nm and 0.252 nm, corresponded to the (002) and (102) lattice planes of ZnO and MoO_3 respectively. The discrete interlayer spacing also verified the single crystalline nature of the MoO_3 coating. The acquired SAED patterns distinctly representing the MoO_3 coating and the ZnO base material are presented in Fig. 6e and f, whereas the diffraction angles, d-spacing and allied parameters of each numbered reflection are arranged in Table 1 and 2 (Supporting information) respectively. The diffractions in the SAED patterns were in close agreement with XRD findings.

As the charge retention and transfer is an essential prerequisite to determining the reactive oxygen species (ROS) generating efficiency of a photocatalyst, therefore, prior to the actual photocatalytic experiments, the synthesized catalysts were subjected to electrochemical impedance (EI) spectroscopy and chronopotentiometry. The Nyquist plots of EI spectra of pure, 0.5, 1, 3 and 5wt% MoO_3 coated ZnO in the dark and under illumination are compared in supporting information of Fig. S1a and b, respectively. The decreased electron transfer resistance for the coated samples as compared to bare ZnO in the dark measurements revealed the facilitating role of MoO_3 coating for the mobility of electrons under external bias (Fig. S1a). From photocatalysis point of view, the electron transfer behavior under illumination is more relevant and can furnish valuable clues regarding the probable performance of the catalysts in the actual photocatalytic experiments. Under illumination, a significant decrease in the diameter of the semi-circular high-frequency region as compared to that of pure ZnO revealed the significantly lower charge transfer resistance of the coated materials. The comparison of the resistance both in the high (semi-circular) and low (linear) predicted the comparable charge transfer ability of 0.5, 1 and 3wt% MoO_3 coated ZnO whereas a comparative increase in the resistance was established for 5wt% MoO_3 coated sample. In terms of photocatalysis, the same may be correlated to the better separation of photogenerated excitons (e^--h^+), extended lifetime of the excited states and expected an enhanced generation of ROS [38]. The charge-discharge curves, in the dark and under illumination, are presented in the supporting information (Fig. S1c and d). The non-ideal charge-discharge curves disclosed the pseudo-capacitative behavior of the electrodes. The deviation from the symmetrical triangular shape is due to the faradaic reaction occurring at the electrode surface [39-41]. The difference in the time span of charge and discharge in the dark and under illumination suggested the varying specific capacitance for each

powder. Based on the comparison, among all the powders, a better charge retaining ability was noticed for of 1wt% MoO_3 coated ZnO. The estimated specific capacitance of 66.5 F g^{-1}, 46.6 F g^{-1}, 58.3 F g^{-1}, 49.9 F g^{-1}, and 48.1 F g^{-1} in the dark and 49.0 F g^{-1}, 52.5 F g^{-1}, 70.6 F g^{-1}, 62.4 F g^{-1}, 53.5 F g^{-1} under illumination for pure, 0.5, 1, 3 and 5wt% MoO_3 coated ZnO respectively. The higher specific capacitance of 1wt% MoO_3 loaded ZnO sample revealed its comparatively high electrical conductivity that can be correlated to efficient charge transfer ability in reference to photocatalytic processes. Although, pure ZnO demonstrated significantly high capacitance in the dark, however, under illumination, decreased significantly due to photocorrosion.

3.2. Photocatalytic removal of chloro-acetic acid derivatives

The photocatalytic activity of the synthesized powders was evaluated for the removal of acetic acid and chloroacetic acid derivatives and monitored the progress of the removal process by ion chromatography (IC) in two different operational modes. The isocratic mode was employed to measure the instantaneous decrease and simultaneous increase in the in the concentration of chloro substrates and released chloride ions, respectively, whereas the complete profiling of all the released anions was accomplished by gradient mode. Prior to sunlight exposure, the dark experiments revealed the varying magnitude of adsorption of substrates on each powder. A ~2.3%, ~7%, ~7.5%, ~5.12% and ~3.6% of MCAA was adsorbed on pure, 0.5, 1, 3 and 5wt% MoO_3 loaded ZnO powders respectively. The representative re-plotted IC profiles for the removal of MCAA over bare ZnO and 1 wt% MoO_3 coated ZnO, as a function of sunlight exposure time, illustrating the time-scale decay and growth of the MCAA and Cl^- peaks, are presented in Fig. S2a and b (Supporting information), respectively. Based on the analysis of respective standards, the peaks observed at the retention time of ~4.91 and ~5.45 mins were assigned to monochloro-acetate (MCAc) and chloride (Cl^-) ions, respectively. Noticeably, in the IC profile of MCAA for pure ZnO (Fig. S2a) an intense peak at ~7.88 mins, in the ascending trend with the increasing sunlight exposure time, is observable that indicated the formation of the stable ionic organic byproduct as a consequence of MCAA degradation. The same was neither observed for 1wt% (Fig. S2b) nor for any other MoO_3 coated ZnO catalyst. The variations in the concentration (ppm) of MCAA and Cl^- ions with the increasing sunlight exposure time, evaluated from the calibration plots of both the ions, are presented in Fig. 7a and b. Although in comparison to pure ZnO, all the MoO_3 coated ZnO powders exhibited significantly high activity for the removal of MCAA however, a marked improvement was noticed for the lower (0.5 and

1wt%) as compared to higher (3 and 5wt%) coating levels (Fig. 7a). The 1wt% MoO_3 catalyst decreased the concentration of MCAA below 1ppm in 180 mins of exposure whereas for 0.5wt% catalyst the same was accomplished in 240 mins of exposure. A further increase in the coating density resulted in the decreased activity. A similar increasing trend was observed in the concentration of Cl^- ions with the increasing sunlight exposure time (Fig. 7b). Additionally, the concentration of released Cl^- ions in solution was consistent with the decrease in the concentration of the MCAA. The bar graph expounding the comparison of the percentage adsorption and degradation of the MCAA substrate as a function of sunlight exposure time is presented in Fig. 7c. In the initial 20 min of sunlight exposure, compared to ~7% for pure ZnO, the 0.5, 1, 3 and 5wt% MoO_3 coated powders removed ~14%, ~18%, ~13% and ~10% of MCAA respectively. Compared to pure ZnO, a ~2.5 fold increase in the removal efficiency of MCAA was noticed for 1wt% MoO_3 loaded catalyst in the initial span of 20 mins. The 0.5 and 1wt% MoO_3 loaded catalysts removed >95% in 180 mins of exposure and only 1% catalyst managed to remove > 99.5% of the substrate in 240 mins of exposure. The comparison of the graphical estimation of the rate constants for the degradation process in the presence of bare and MoO_3 coated ZnO catalysts, evaluated by plotting the $\ln(C_o/C)$ versus the exposure time, is presented in Fig. 7d. Initially, until 120 min of exposure, the rate of MCAA removal increased linearly followed by an exponential increase afterward. Probably with the decreasing concentration the ratio of the ROS to MCAA molecules has increased that results in the rapid depletion of the substrate. Interestingly, the magnitude of the deviation from Langmuir-Hinshelwood kinetic model was more pronounced for the relatively active catalysts loaded with a lower concentration of MoO_3. Compared to ~60% decrease in the concentration of MCAA for pure ZnO, a TOC removal of ~12% for ZnO was witnessed that indicated the transformation of MCAA to some other compound rather than mineralization. Therefore, as degradation can result due to any structural change in the substrate molecule, the removal efficiency of a photocatalyst cannot be accurately judged on the basis of degradation measurements only without coupling with the mineralization (TOC removal) data. The 0.5wt% MoO_3 loaded ZnO catalyst removed 77% of the TOC in 240 min of sunlight exposure, whereas ~89% TOC was removed by 1wt% MoO_3 loaded ZnO in the same span of time. A decreasing trend in the TOC removal was witnessed with the increasing coating density. Interestingly, the mineralization process followed the Langmuir-Hinshelwood kinetic model with acceptable correlation.

The representative IC degradation profiles for the degradation of dichloroacetic acid (DCAA) over pure and 1wt% MoO_3 coated ZnO are compared in Fig. S3a and b (Supporting information). The DCAA in the ionic form was eluted at the retention time of ~6.19 min for both the catalysts whereas the released Cl^- ions appeared at ~5.45 min. In the dark experiments, a low adsorption of ~2.1%, ~7.6%, ~9.4%, ~7.4% and ~4.9% of DCAA on pure, 0.5, 1, 3 and 5wt% MoO_3 coated ZnO powders, respectively, was noticed. The degradation of DCAA in the presence of ZnO revealed the similar practice as that observed for MCAA with the appearance of an additional peak of the degradation products at ~8.02 min. For MCAA the same was observed at ~7.88 min. The marked variation in the evaluation times recognized both the products as dissimilar entities. The comparison of the percentage degradation of DCAA as a function of the sunlight exposure time is presented in Fig. S3c. Compared to MCAA, the removal of DCAA was significantly swift for all the catalysts including pure ZnO. A percentage degradation of ~28%, ~52%, ~69% and ~82% was observed for pure ZnO in 60, 120, 180 and 240 min of sunlight exposure whereas, ~16%, ~30%, ~43% and ~58% of MCAA was noticed in the same period. Although, the decrease in the intensity of the DCAA peak indicated the degradation of the substrate, however, similar to the MCAA degradation, the successive growth of the corresponding by-product peak in the retention time region of 8-8.5 min (Fig. S3a) verified the transformation rather than degradation. The minor TOC removal of ~10.4% further verified the finding. The successively growing intense by-product peak, as observed for pure ZnO, was not experiential in the IC profiles of the coated catalysts. Among the coated catalysts, the 0.5, 1 and 3wt% MoO_3@ZnO showed the significantly enhanced activity for the degradation of DCAA while the activity of 5wt% MoO_3@ZnO was marginally higher than that of pure ZnO. Although comparable with 0.5wt% MoO_3@ZnO, the optimum activity was observed for 1wt% MoO_3 coated ZnO as compared to ~97% for 0.5wt%, ~99.5% removal of the substrate was witnessed for 1wt% MoO_3 coated ZnO in 180 mins of exposure. The plots of $\ln(C_o/C)$ versus the sunlight exposure time revealed the deviation from the Langmuir-Hinshelwood kinetic model. The magnitude of the deviation was significantly higher for 0.5 and 1wt% MoO_3 loaded catalysts whereas a mild deviation was observed for pure ZnO, 3 and 5wt% MoO_3@ZnO. The changes in the concentration of chloride ions as a function of the sunlight exposure time, for all the catalysts under study, are compared in Fig. S3d. Similar to MCAA removal, the increase in the concentration of chloride ions consistent with the disappearance of the substrate predicted the

synchronization between the two processes. As the number of Cl groups in DCAA is twice as compared to MCAA, an expected higher concentration of Cl^- ions in the solution was noticed. A significantly high TOC removal of ~90% was observed for 1wt% MoO_3@ZnO catalyst as compared to 15% for pure ZnO. Additionally, the rate of TOC removal for DCAA was significantly higher than that of the MCAA. The difference in both the degradation as well as mineralization of MCAA and DCAA may be associated with the higher number of Cl groups.

The successive decrease in the luminescence intensity with the increasing coating level (Fig. 1e) predicted the efficient suppression of recombination process, however, the lower activity for the removal of substrates elucidated the inability of the higher coating levels to deliver the excitons to the reductants that rationalized the limitations of the PL analysis regarding the prediction of charge transport in actual photocatalytic performance. On the other hand, the comparison of the electrochemical behavior in the dark and under illumination estimated by EIS (Fig. S1a and b) and charge-discharge (Fig. S1c and d) furnishes valuable information regarding the charge trapping and transfer process.

As the coated catalysts were synthesized by gradually concentrating the Mo^{6+} ions at the surface of pre-synthesized ZnO by slow thermal evaporation, it might be presumed that at lower concentrations (0.5 and 1wt%), patches of MoO_3 are formed by the initial attachment of Mo^{6+} ions with the singly charged surface oxygen that serves as trap and transfer sites for the excited electrons. Additionally, at lower Mo^{6+} concentrations (≤ 1wt%) due to the partial surface coverage, the contribution of the MoO_3 patches in the absorption of incident photons is significantly lower. On the other hand, at higher Mo^{6+} loading (≥ 3wt%) the singly charged surface oxygen groups are exhausted that results in the complete ZnO surface coverage by the successive layers of MoO_3. The same is observable in the FESEM and TEM analysis (Fig. 5 and 6).

Although a variety of ROS are generated in the form of a cascade, in the aerated aqueous photocatalytic system, however, the survival of superoxide anion ($O_2^{\bullet -}$) and hydroxyl ($^{\bullet}OH$) radicals has been reported for prolonged periods [42]:

$$O_2(dissolved) + e_{cb}^- \rightarrow O_2^{\bullet -} \quad (1)$$

$$H_2O(adsorbed) + h_{vb}^+ \rightarrow HO^{\bullet} + H^+ \quad (2)$$

Besides many other physicochemical factors [42], the suitability of the electrochemical potentials established across the valence and conduction bands in the aqueous medium is also vital in regulating the population of superoxide anion ($O_2^{\bullet -}$) and hydroxyl ($^{\bullet}OH$) radicals. In the current study, though, the accelerated degradation of MCAA and DCAA substrates with the corresponding release of Cl^- ions in the solution predicted the possible involvement of charged ROS ($O_2^{\bullet -}$) in the removal process, the suitability of the conduction band edges for the generation of superoxide anion radicals was investigated by measuring the flat band potential (V_{fb}). The Mott-Schottky plots extracted from SPIES analysis of pure ZnO, MoO_3 and the synthesized coated powders at neutral pH in the dark and under illumination are presented in Fig. 8a and b, where the prevalence of the negative potential regions signified the n-type nature of the materials. Compared to the dark measurements (Fig. 8a), except for the decreased intensity representing the better electron transport, no significant change in the shapes of the curves was observable under illumination (Fig. 8b). The graphical evaluation of the V_{fb} from the extrapolation of the linear portion of the curves in the negative potential region to the x-axis, in the dark and under illumination, is presented in Fig. 8c and d. As the V_{fb} of a n-type semiconductor corresponds to the potential of the conduction band edge [43] the evaluated V_{fb} values were regarded as the conduction band potentials (V_{cb}) of the materials. The evaluated V_{fb} values of -0.31 V for pure ZnO were in accordance with the literature values, however, that of -0.42 V for pure MoO_3 was significantly deviated [44, 45]. In the coated powders, a strong influence on V_{fb} was noticed with the increasing MoO_3 coating where except for 0.5wt% coated catalyst, the onsets were shifted to more negative values. The V_{fb} of -0.30 V for 0.5wt% MoO_3 coated powder was merely the same as ZnO. The evaluated V_{fb} values for 1, 3 and 5wt% MoO_3 coated ZnO were -0.60 V, -0.62V, and -0.65 V, respectively. Under illumination, the V_{fb} for all the powders including ZnO and MoO_3 was shifted to more negative values. The negative V_{fb} values support the instantaneous ample generation of superoxide anion ($O_2^{\bullet -}$) radicals in the system. The suitability of V_{fb} values and the release of the significantly high concentration of Cl^- ions, being negatively charged in nature, categorically support the major involvement of charged rather than neutral ROS in the degradation process. Additionally, some recent studies have also questioned the existence and involvement of hydroxyl radicals in the oxidation process and proposed a complex route based on pH for their generation [42]. On the other hand, the mobility,

diffusion and the reactivity of the superoxide anion ($O_2^{\bullet-}$) radicals in the aqueous medium are also well established [46, 47].

The trichloroacetic acid (TCAA) also exhibited low average adsorption of ~5% on all the catalysts. The time-scale IC profiles for the degradation TCAA in the presence of pure and 1wt% MoO_3 coated ZnO are presented in Fig. 9a and b, where due to the enhanced dissociation under the influence of the catalysts, a shift in the peak position of the TCAA is observable. The shift was more pronounced for the coated catalyst as compared to pure ZnO. The comparison of IC profiles of TCAA removal over TiO_2 (Degussa P-25) is also presented in Fig.9c. Interestingly, as presented, a similar response was observed with TiO_2 (Degussa P-25). Fig. 9d shows the assessment of TCAA removal over bare, 1 wt% MoO_3 coated ZnO and TiO_2 (Degussa P-25) powders. A mild degradation of ~5%, ~12%, and ~15% was noticed for pure ZnO, 1wt% MoO_3 coated ZnO and TiO_2 (Degussa P-25) respectively. Additionally, the negligible TOC removal and release of Cl^- ions was also observable.

To explore the probable reasons of the low degradation of the TCAA as compared to MCAA and DCAA the chemical configuration of the derivatives was analyzed. The stereochemical structures of MCAA, DCAA and TCAA are presented in Supporting information (Fig. S4). In CAA derivatives, the electronegative Cl groups at the terminal position induce charge polarization in the C-Cl thus imparting a partial positive charge on the attached carbon atom that serves as the interaction site for the incoming negatively charged superoxide anion ($O_2^{\bullet-}$) radicals. The corresponding yield of Cl^- ions in the solution during the course of the degradation process also substantiate the displacement of Cl groups by the negatively charged superoxide anion radicals as the origination of the degradation process. An increase in the magnitude of the partial positive charge on the terminal carbon atom might be expected with the increasing number of Cl groups with the enhanced degradation and significantly higher yield of chloride ions in the solution. Based on the trend observed in the degradation of MCAA and DCAA, as per analogy, a comparatively swift degradation of TCAA was expected, however, the apparent low degradation indicated the influence of stereochemical factors such as the size and orientation of the Cl groups that affect the interaction of the ROS with TCAA besides the enhanced polarity induced by Cl groups.

To investigate it further, the geometry of the derivatives was optimized by HyperChem (8.0.10) with the provision of the electrostatic charge distribution. The lowest energy

configurations of the chloroacetic acid derivatives with the extended charge distribution are presented in Supporting information (Fig. S5). The comparison of the optimized structures revealed the successive increase in the magnitude of the electronic shielding of the terminal carbon with the increasing number of Cl groups. For MCAA and DCAA, with the presence of smaller sized electron deficient H atoms (~0.053 nm), the terminal carbon atom with the partial positive charge remains accessible to negatively charged superoxide radicals that results in the degradation as well as mineralization whereas for TCAA, the bulky electron rich Cl groups (~0.181 nm) completely entrap the terminal carbon atom making it inaccessible to the incoming charged ROS. As the electronic cloud of the chloride groups, due to the orientation, repels back the interacting negatively charged $O_2^{\bullet -}$ radicals, therefore, unable to contribute to the degradation of the TCAA. These findings further strengthen the experimental evidence that supports the superoxide anion ($O_2^{\bullet -}$) radicals are the major contributors in the degradation as well as mineralization process. The observed mild degradation of the TCAA is probably due to the interaction of neutral ROS most likely the hydroxyl radicals. The investigation was further extended and the degradation of the pure acetic acid (AA) was examined under the identical conditions. The IC profiles for the removal of AA over pure ZnO, 1wt% MoO_3 coated ZnO, and TiO_2 (Degussa P-25) is presented in the Supporting information (Fig. S6a-c). As AA is highly dissociative in the aqueous medium no shift in the peak position was noticed under the influence of catalysts. The comparison of the percentage degradation with the increasing sunlight exposure time is presented in the supporting material (Fig. S6d). The degradation of AA was comparatively higher than TCAA on both the catalysts but significantly lower than that of MCAA and DCAA. The pure ZnO degraded ~9% of AA in 240 mins of exposure, whereas 1wt% MoO_3 coated ZnO and TiO_2 (Degussa P-25) removed ~20% and ~25% of the substrate in the same period. With the mild increase, the degradation of AA followed the similar trend as that of the TCAA. The major difference between the AA and TCAA are the substituents attached to the terminal carbon atom. The H groups are of smaller size (53 pm) and an electron deficient ($1s^1$) with a low electronegativity of 2.2 for the shared electron pair whereas the Cl groups are bulky (181 pm), electron rich ($3s^2\ 3p^5$) with the significantly high electronegativity of 3.16. The H groups of AA have neither the potential to induce charge separation nor the ability to shield the terminal carbon, whereas the Cl groups of TCAA have both the characteristics. Therefore, the degradation of TCAA is retarded by the shielding of the terminal carbon by the Cl groups

while for AA the same was observed due to the non-existence of a sufficient polarity to facilitate the negatively charged $O_2^{\bullet -}$ radicals. The minor degradation of AA is either accomplished due the minor polarity induced by the COO^- groups or by the neutral hydroxyl radicals. Therefore, for MCAA and DCAA, the Cl group/s induced polarity facilitates the interaction of the superoxide anion radicals whereas the shielding of the terminal carbon by the bulky Cl groups in TCAA and lack of enough polarity in AA retard the degradation process. A similar behavior of TCAA has already been reported in the literature where no hydrogen evolution was observed in the presence of TCAA over Pt/TiO_2 surfaces [48].

The possible role of $O_2^{\bullet -}$ radicals and the probable mechanism of degradation process was further investigated by examining the degradation pattern in the absence of oxygen and analyzing the released ions during the degradation of MCAA and DCAA. The comparison of the degradation (%) and the C/C_o plots for the degradation of MCAA over 1 wt% MoO_3 coated ZnO with and without dissolved O_2 is presented in Fig. 10a and b respectively, whereas the time scale IC profile in the absence of O_2 is presented in the Supporting information (Fig. S7). A substantial decrease in the removal of MCAA pointed the foremost role of dissolved O_2, as removed by argon (Ar) purging, in the degradation process. The nearly negligible decrease in the concentration of MCAA, in the initial 90 min of exposure, specified the non-formation of $O_2^{\bullet -}$ radicals due to the absence of dissolved O_2. As the adsorbed H_2O oxidation by the holes (h^+) leads to the *in-situ* generation of O_2, a gradual acceleration in the degradation process was witnessed afterward. The initial mild decrease in MCAA concentration of MCAA is probably due to the direct interaction of the substrate with the photo-generated entities in competition with adsorbed water molecules. The typical ion chromatograms acquired during the removal of MCAA and DCAA in the presence of 1 wt% MoO_3 coated ZnO under identical experimental conditions are presented in Fig. 10c and d. The appeared ions in both the chromatograms were identified by comparing with the standards. In the degradation of both MCAA and DCAA besides the substrates and Cl^- ions, the other identified ions were ClO_2^-, ClO_3^-, ClO_4^-, CO_3^{2-} and $C_2O_4^{2-}$. The oxalate anions can be formed as a result of the oxidative coupling of the carbon entities generated as a consequence of the displacement of a single Cl group/s of MCAA and DCAA by $O_2^{\bullet -}$ radicals. A successive increase in the concentration of $C_2O_4^{2-}$ ions was noticed during the degradation of the MCAA. An increase in the concentration followed by a decrease for DCAA indicated the enhanced interaction of ROS with of $C_2O_4^{2-}$ with the decreasing

concentration of the substrate. The identification of the oxidation products of chloride ions in the profiles, both in the degradation of MCAA and DCAA, confirmed the further oxidation of the released chloride ions either by the excitons or the ROS. The formation of CO_3^{2-} ions in the mineralization of organic compounds is the highly expected product. Keeping in view the suitability of the conduction band edges, the probability of the ROS that is generated by the current system and the chemical features associated with the substrates, the plausible routes of the degradation of MCAA, DCAA and TCAA are proposed in scheme 1.

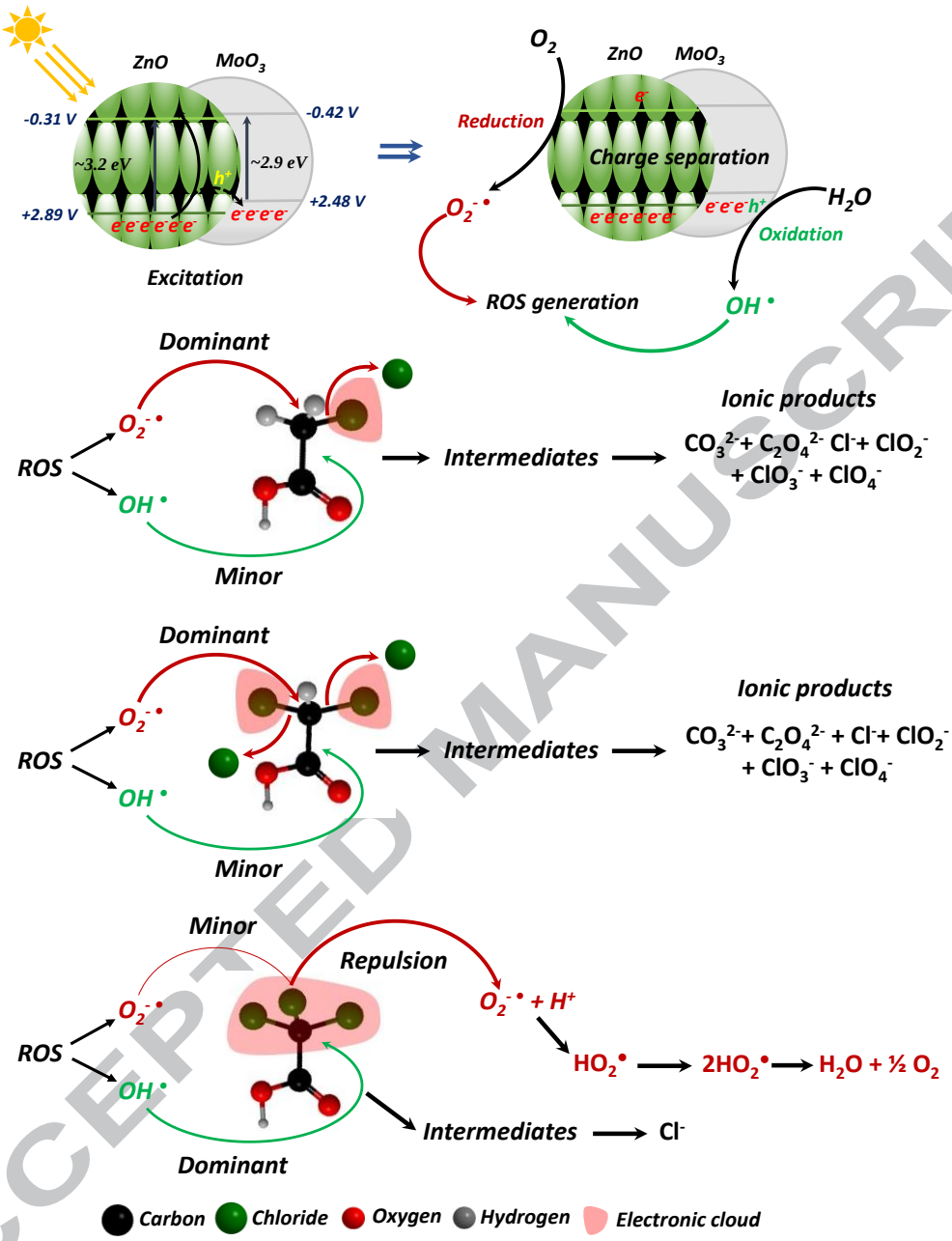

Scheme 1: The plausible routes of chloro-acetic acid derivatives degradation/mineralization over 1wt% MoO_3 coated ZnO in sunlight exposure.

Although hydroxyl radicals ($OH^{\bullet}$) have been described as the major oxidizers in various photocatalytic processes [49-51], however, the current study, verified the majority involvement of superoxide anion radicals (Scheme 1). In the current study, the photonic efficiencies (PEs) for the removal of MCAA and DCAA were evaluated by altering the relation reported in the literature [52]. The comparison of the PEs for the removal of MCAA and DCAA in the sunlight exposure over pure and MoO_3 coated ZnO powders is presented in Fig. 10e and f. For MCAA, the slow degrading catalysts i.e. ZnO and 5 wt% MoO_3 coated ZnO exhibited the persistent average PEs during the exposure time of 240 mins and the average efficiencies of ~1.11% and ~1.60% were evaluated. On the other hand, a sharp increase in PEs in the initial 20 mins of exposure followed by the gradual decrease was noticed for 0.5, 1 and 3 wt% MoO_3 coated ZnO with the maximum PEs of ~2.75, ~3.74 and ~2.39% respectively. Contrary to MCAA, except for ZnO, after attaining the maximum value in the initial 20 min of exposure, a sharp decrease in the PEs was noticed for all the catalysts. Interestingly, the observed maximum photonic efficiencies of ~4.80, ~6.5, ~3.0 and ~3.6% for 0.5, 1, 3 and 5 wt% MoO_3 coated ZnO in the initial 20 mins of exposure were significantly higher than that for MCAA. These PEs values are in good agreement with the previously reported literature values [53, 54]. It might be anticipated that the decrease in the photonic efficiencies with the increasing exposure time is owing to the depleting concentration due to rapid removal that disturbs the accessibility between the excitons and the substrate molecules, whereas the significantly enhanced efficiencies for the removal of DCAA signifies the supporting role of the Cl groups in the degradation process and further augment the proposed mechanism.

The stability of pure and MoO_3 coated ZnO powders under illumination was evaluated by cyclic voltammetric analysis. The analysis was performed in a potential range of -0.5 to -1.55 V (vs. Ag/AgCl/saturated) at a sweep rate of 100 mVs^{-1} in the dark and under illumination. The cyclic voltammetric behavior of the powders in the dark is presented in the Supporting information (Fig. S8a). The CVs of all the modified electrodes exhibited almost similar patterns in the dark and their profiles revealed an electrochemical pseudo-capacitive behavior, characteristic of redox reactions. The CVs in the dark exhibited an oxidation peak at -1.18 V in the forward scan due to the formation of $Zn(OH)_4^{2-}$ ions under applied potential whereas the corresponding reduction peak in the reverse scan at -1.33 V represented the reduction of the soluble zincate species present in the solution. For 0.5, 1, 3 and 5wt% MoO_3 coated ZnO

electrodes, in addition to the decrease in the oxidation peak current, a considerable shift in the oxidation peak potential was also observed. The shifting of the peak potential is probably due to the possible changes occurred to the surface morphology of ZnO after modification with Mo^{6+}. Additionally, the surface MoO_3 may have a contributory role in this regard. A significant decrease in the reduction peak current depicted the decreased release of $Zn(OH)_4^{2-}$ (zincate ion) in the solution due to the surface coating. The estimation of the suppression of the photocorrosion of ZnO, under illumination, by cyclic voltammetry, is well established [55, 56]. As presented in the Supporting information (Fig. S8b), compared to uncoated ZnO, the reduced magnitude of zincate ion release and its corresponding reduction peak was more prominent for the coated samples under illumination. The appearance of the additional peak under illumination at -1.05 V showed the tendency of dissolution of uncoated ZnO with the release of Zn^{2+} ions. The complete disappearance of the same demonstrated the effectiveness of the MoO_3 coating in inhibiting the self-oxidation of ZnO by the photogenerated positive entities with the release Zn^{2+} ions. The performance of the 1wt% MoO_3@ZnO catalyst in the successive use for three consecutive cycles for the removal of the MCAA and DCAA is shown in Supporting information (Fig. S9). The catalyst exhibited sustained activity for the removal of both MCAA and DCAA.

4. Conclusions

The study revealed the efficacy of MoO_3 surface coating in effectively suppressing the e^--h^+ recombination process and protecting ZnO against photocorrosion. The lower coating levels of MoO_3 significantly enhanced the photocatalytic activity to ZnO whereas a detrimental effect was observed at higher levels. The suitability of the band edge positions of ZnO and MoO_3 and the evidences conceived from the time-scale chemical analysis proposed superoxide anions as the majority oxidizers in the degradation process. The polarity induced by the Cl groups facilitates the interaction of the superoxide anion radicals in the removal of MCAA and DCAA whereas the shielding of the polarity induced terminal carbon by the Cl groups in TCAA and lack of enough polarity in AA retard the degradation process. The released chloride ions further interact either with excitons or the ROS to form ClO_2^-, ClO_3^- and ClO_4^- during the degradation process.

Acknowledgements

A. Hameed, M. Aslam, M.T. Qamar and Iqbal M.I. Ismail are thankful to Center of Excellence in Environmental Studies (CEES), King Abdulaziz University and Ministry of Higher Education (MoHE), KSA, for support. M. T. Qamar also gratefully acknowledges the support from Chemistry Department, Faculty of Science, King Abdulaziz University, KSA.

References

1. C. Yu, W. Zhou, H. Liu, Y. Liu, D.D. Dionysiou, Design and fabrication of microsphere photocatalysts for environmental purification and energy conversion, Chem. Eng. J. 287 (2016) 117-129.
2. J.E. Casillas, F. Tzompantzi, S.G. Castellanos, G. Mendoza-Damián, R. Pérez-Hernández, A. López-Gaona, A. Barrera, Promotion effect of ZnO on the photocatalytic activity of coupled Al_2O_3-Nd_2O_3-ZnO composites prepared by the sol-gel method in the degradation of phenol, Appl. Catal. B: Environ. 208 (2017) 161-170.
3. M. Aslam, I.M.I. Ismail, T. Almeelbi, N. Salah, S. Chandrasekaran, A. Hameed, Enhanced photocatalytic activity of V_2O_5-ZnO composites for the mineralization of nitrophenols, Chemosphere, 117 (2014) 115-123.
4. I.K. Konstantinou, T.A. Albanis, TiO_2-assisted photocatalytic degradation of azo dyes in aqueous solution: kinetic and mechanistic investigations: a review, Appl. Catal. B: Environ. 49 (2004) 1-14.
5. M.N. Chong, B. Jin, C.W.K. Chow, C. Saint, Recent developments in photocatalytic water treatment technology: a review, Water Res. 44 (2010) 2997-3027.
6. J. Schneider, M. Matsuoka, M. Takeuchi, J. Zhang, Y. Horiuchi, M. Anpo, D.W. Bahnemann, Understanding TiO_2 photocatalysis: mechanisms and materials, Chem. Rev. 114 (2014) 9919–9986.
7. C. Yu, Z. Wu, R. Liu, D.D. Dionysiou, K. Yang, C. Wang, H. Liu, Novel fluorinated Bi_2MoO_6 nanocrystals for efficient photocatalytic removal of water organic pollutants under different light source illumination, Appl. Catal. B: Environ. 209 (2017) 1-11.

8. A.L. Linsebigler, G. Lu, J.T. Yates, Photocatalysis on TiO_2 surfaces: principles, mechanisms, and selected results, Chem. Rev. 95 (1995) 735–758.

9. C. Yu, W. Zhou, L. Zhu, G. Li, K. Yang, R. Jin, Integrating plasmonic Au nanorods with dendritic like α-Bi_2O_3/$Bi_2O_2CO_3$ heterostructures for superior visible-light-driven photocatalysis, Appl. Catal. B: Environ. 184 (2016) 1-11.

10. K. Nakata, A. Fujishima, TiO_2 photocatalysis: design and applications, J. Photochem. Photobiol. C: Photochem. Rev. 13 (2012) 169–189.

11. S.G. Kumar, L. Gomathi Devi, Review on Modified TiO_2 Photocatalysis under UV/Visible Light: Selected Results and Related Mechanisms on Interfacial Charge Carrier Transfer Dynamics, J. Phys. Chem. A 115 (2011) 13211–13241.

12. A. Fujishima, X. Zhang, D.A. Tryk, TiO_2 photocatalysis and related surface phenomena, Surf. Sci. Rep. 63 (2008) 515–582.

13. M.D. Hernández-Alonso, F. Fresno, S. Suárez, J.M. Coronado, Development of alternative photocatalysts to TiO_2: Challenges and opportunities, **Energy Environ. Sci.** 2 (2009) 1231-1257.

14. S. Sakthivel, B. Neppolian, M.V. Shankar, B. Arabindoo, M. Palanichamy, V. Murugesan, Solar photocatalytic degradation of azo dye: comparison of photocatalytic efficiency of ZnO and TiO_2, Sol. Energ. Mat. Sol. Cells 77 (2003) 65–82.

15. S.G. Kumar, K.S.R. Koteswara Rao, Zinc oxide based photocatalysis: tailoring surface-bulk structure and related interfacial charge carrier dynamics for better environmental applications, RSC Adv. 5 (2015) 3306−3351.

16. V. Vaiano, M. Matarangolo, O. Sacco, D. Sannino, Photocatalytic treatment of aqueous solutions at high dye concentration using praseodymium-doped ZnO catalysts, Appl. Catal. B: Environ. 209 (2017) 621-630.

17. A. Hameed, T. Montini, V. Gombac, Photocatalytic decolourization of dyes on NiO–ZnO nano-composites, P. Fornasiero, **Photochem. Photobiol. Sci.** 8 (2009) 677-682.

18. M.T. Qamar, M. Aslam, I.M.I. Ismail, N. Salah, A. Hameed, The assessment of the photocatalytic activity of magnetically retrievable ZnO coated γ-Fe_2O_3 in sunlight exposure, Chem. Eng. J. 283 (2016) 656-667.

19. M. Aslam, I.M.I. Ismail, S. Chandrasekaran, T. Almeelbi, A. Hameed, The suitability of Ce^{3+}-modified ZnO photocatalyst for the mineralization of monochlorophenol isomers in sunlight exposure, RSC Adv. 2 (2014) 49347–49359.

20. S. Rehman, R. Ullah, A.M. Butt, N.D. Gohar, Strategies of making TiO_2 and ZnO visible light active, J. Hazard. Mater. 170 (2009) 560–569.

21. J. Wang, Y. Xia, H. Zhao, G. Wang, L. Xiang, J. Xu, S. Komarneni, Oxygen defects-mediated Z-scheme charge separation in g-C_3N_4/ZnO photocatalysts for enhanced visible-light degradation of 4-chlorophenol and hydrogen evolution, Appl. Catal. B: Environ. 206 (2017) 406-416.

22. K.M. Lee, C.W. Lai, K.S. Ngai, J.C. Juan, Recent developments of zinc oxide based photocatalyst in water treatment technology: a review, Water Res. 88 (2016) 428–448.

23. A. Hameed, M. Aslam, I.M.I. Ismail, S. Chandrasekaran, M.W. Kadi, M.A. Gondal, Sunlight assisted photocatalytic mineralization of nitrophenol isomers over W^{6+} impregnated ZnO, Appl. Catal. B Environ. 160-161 (2014) 227–239.

24. B. Zhao, X. Wang, H. Shang, X. Li, W. Li, J. Li, W. Xia, L. Zhou, C. Zhao, Degradation of trichloroacetic acid with an efficient Fenton assisted TiO_2 photocatalytic hybrid process: Reaction kinetics, byproducts and mechanism, Chem. Eng. J. 289 (2016) 319–329.

25. Y. Li, Y. Xie, S. Peng, G. Lu, S. Li, Photocatalytic hydrogen generation in the presence of chloroacetic acids over Pt/TiO_2, Chemosphere 63 (2006) 1312–1318.

26. M.D. Esclapez, I. Tudela, I.D. García, V. Sáez, P. Bonete, Towards the complete dechlorination of chloroacetic acids in water by sonoelectrochemical methods: Effect of the cathode material on the degradation of trichloroacetic acid and its degradation by-products, Appl. Catal. B: Environ. 166-167 (2015) 66–74.

27. E. Malliarou, C. Collins, N. Graham, M.J. Nieuwenhuijsen, Haloacetic acids in drinking water in the United Kingdom, Water Res. 39 (2005) 2722– 2730.

28. S.W. Krasner, H.S. Weinberg, S.D. Richardson, S.J. Pastor, R. Chinn, M.J. Sclimenti, G.D. Onstad, A.D. Thruston Jr., Occurrence of a new generation of disinfection byproducts, Environ. Sci. Technol. 40 (2006) 7175–7185.

29. J.G. Pressman, S.D. Richardson, T.F. Speth, R.J. Miltner, M.G. Narotsky, E.S. Hunter III, G.E. Rice, L.K. Teuschler, A. McDonald, S. Parvez, S.W. Krasner, H.S. Weinberg, A.B. McKague, C.J. Parrett, N. Bodin, R. Chinn, C.F.T. Lee, J.E. Simmons, Developmental Toxicity Evaluations of Whole Mixtures of Disinfection By-products using Concentrated Drinking Water in Rats: Gestational and Lactational Effects of Sulfate and Sodium, Environ. Sci. Technol. 44 (2010) 7184–7192.

30. C.L. Chun, R.M. Hozalski, W.A. Arnold, Degradation of drinking water disinfection byproducts by synthetic goethite and magnetite, Environ. Sci. Technol. 39 (2005) 8525–8532.

31. H. Czili, A. Horváth, Photodegradation of chloroacetic acids over bare and silver-deposited TiO_2: Identification of species attacking model compounds, a mechanistic approach, Appl. Catal. B: Environ. 89 (2009) 342–348.

32. J. Zhou, Y. Han, W. Wang, Z. Xu, H. Wan, D. Yin, S. Zheng, D. Zhu, Reductive removal of chloroacetic acids by catalytic hydrodechlorination over Pd/ZrO_2 catalysts, Appl. Catal. B: Environ. 134-135 (2013) 222–230.

33. M.T. Qamar, M. Aslam, I.M.I. Ismail, N. Salah, A. Hameed, Synthesis, characterization, and sunlight mediated photocatalytic activity of CuO coated ZnO for the removal of nitrophenols, ACS Appl. Mater. Interfaces 7 (2015) 8757-8769.

34. M. Aslam, M.T. Qamar, M.T. Soomro, I.M.I. Ismail, Z.A. Rehan, M.W. Ashraf, A. Hameed, The effect of cerium alteration on the photocatalytic performance of WO_3 in sunlight exposure for water decontamination, RSC Adv. 6 (2016) 2436–2449.

35. Y. Xu, M.A.A. Schoonen, The absolute energy positions of conduction and valence bands of selected semiconducting minerals, Am. Mineral. 85 (2000) 543–556.

36. M.T. Qamar, M. Aslam, Z.A. Rehan, M.T. Soomro, J.M. Basahi, I.M.I. Ismail, A. Hameed, The effect of Fe^{3+} based visible light receptive interfacial phases on the photocatalytic activity of ZnO for the removal of 2,4-dichlorophenoxy acetic acid in natural sunlight exposure, Sep. Purif. Technol. 172 (2017) 512–528.

37. Q.Y. Bao, J.P. Yang, Y.Q. Li, J.X. Tang, Electronic structures of MoO_3-based charge generation layer for tandem organic light-emitting diodes, Appl. Phys. Lett. 97 (2010) 063303-3.

38. M. Aslam, M.T. Qamar, M.T. Soomro, I.M.I. Ismail, N. Salah, T. Almeelbi, M.A. Gondal, A. Hameed, The effect of sunlight induced surface defects on the photocatalytic activity of nanosized CeO_2 for the degradation of phenol and its derivatives, Appl. Catal. B: Environ. 180 (2016) 391-402.

39. S. Nagamuthu, S. Vijayakumar, G. Muralidharan, Ag incorporated Mn_3O_4/AC nanocomposite based supercapacitor devices with high energy density and power density, Dalton Trans. 43 (2014) 17528-17538.

40. Y.Z. Zhang, J. Zhao, J. Xia, L. Wang, W.Y. Lai, H. Pang, W. Huang, Room temperature synthesis of cobalt-manganese-nickel oxalates micropolyhedrons for high-performance flexible electrochemical energy storage device, Sci. Rep. 5 (2015) 8536.

41. S.K. Meher, P. Justin, G. Ranga Rao, Nanoscale morphology dependent pseudocapacitance of NiO: Influence of intercalating anions during synthesis, Nanoscale 3 (2011) 683-692.

42. P. Pichat, Photocatalysis and Water Purification: From Fundamentals to Recent Applications, first ed. Wiley-VCH Verlag, Weinheim, Germany, 2013.

43. D. Hwang, J. Kim, T. Park, J. Lee, Mg-Doped WO_3 as a Novel Photocatalyst for Visible Light-Induced Water Splitting, Catal. Lett. 80 (2002) 53-57.

44. Y. He, L. Zhang, X. Wang, Y. Wu, H. Lin, L. Zhao, W. Weng, H. Wan, M. Fan, Enhanced photodegradation activity of methyl orange over Z-scheme type MoO_3–g-C_3N_4 composite under visible light irradiation, RSC Adv. 4 (2014) 13610-13619.

45. T. Liu, B. Li, Y. Hao, Z. Yao, MoO_3-nanowire membrane and $Bi_2Mo_3O_{12}/MoO_3$ nano-heterostructural photocatalyst for wastewater treatment, Chem. Eng. J. 244 (2014) 382–390.

46. B.G. Kwon, J. Yoon, Experimental evidence of the mobility of hydroperoxyl/superoxide anion radicals from the illuminated TiO_2 interface into the aqueous phase, Bull. Korean Chem. Soc. 30 (2009) 667–670.

47. B.G. Kwon, J.O. Kim, J.K. Kwon, An Advanced Kinetic Method for $HO_2^{\bullet}/O_2^{-\bullet}$ Determination by Using Terephthalate in the Aqueous Solution, Environ. Eng. Res. 17 (2012) 205–210.

48. Y. Li, Y. Xie, S. Peng, G. Lu, S. Li, Photocatalytic hydrogen generation in the presence of chloroacetic acids over Pt/TiO_2, Chemosphere 63 (2006) 1312–1318.

49. M.R. Hoffmann, S.T. Martin, W. Choi, D.W. Bahnemann, Environmental applications of semiconductor photocatalysis, Chem. Rev. 95 (1995) 69-96.

50. D.F. Ollis, H. Al-Ekabi, (Eds.), Photocatalytic Purification and Treatment of Water and Air, Elsevier, Amsterdam, 1993.

51. N. Serpone, E. Pelizzetti, (Eds.), Photocatalysis, Fundamentals and Applications, Wiley, New York, 1989.

52. I.E. Wachs, S.P. Phivilay, C.A. Roberts, Reporting of reactivity for heterogeneous photocatalysis, ACS Catal. 3 (2013) 2606−2611.

53. M.J. Muñoz-Batista, A. Kubacka, A.B. Hungría, M. Fernández-García, Heterogeneous photocatalysis: Light-matter interaction and chemical effects in quantum efficiency calculations, J. Catal. 330 (2015) 154–166.

54. N. Serpone, J. Martin, S. Horikoshi, H. Hidaka, Photocatalyzed oxidation and mineralization of C1–C5 linear aliphatic acids in UV-irradiated aqueous titania dispersions—kinetics, identification of intermediates and quantum yields, J. Photochem. Photobiol. A Chem. 169 (2005) 235–251.

55. M. Aslam, M.T. Soomro, I.M.I. Ismail, N. Salah, M.A. Gondal, A. Hameed, Sunlight mediated removal of chlorophenols over tungsten supported ZnO: electrochemical and photocatalytic studies, J. Environ. Chem. Eng. 3 (2015) 1901-1911.

56. M.T. Qamar, M. Aslam, Z.A. Rehan, M.T. Soomro, J.M. Basahi, I.M.I. Ismail, T. Almeelbi, A. Hameed, The influence of p-type Mn_3O_4 nanostructures on the photocatalytic activity of ZnO for the removal of bromo and chlorophenol in natural sunlight exposure, Appl. Catal. B: Environ. 201 (2017) 105–118.

Figure Captions

Figure 1. The comparison of (a) the DR spectra in the range of 200 to 900 nm (b) the solid-state absorption spectra in 300 to 800 nm range. The graphical evaluation of the band edges (c) ZnO, MoO_3, 0.5 and 1 wt% MoO_3 coated ZnO (d) ZnO, 3 and 5 wt% MoO_3 coated ZnO whereas (e) and (f) compares the PL and Raman spectra of bare ZnO and MoO_3 coated ZnO powders respectively.

Figure 2. The comparison of (a) XRD patterns of ZnO, MoO_3, and MoO_3 coated ZnO in the 2θ range of 20º to 80º (b) the exploded view from 2θ = 20° to 2θ = 30° showing the growth of the reflections due to the MoO_3 coating and respective *hkl* indices.

Figure 3. The comparison of wide angle survey scans of 3 wt% MoO_3 coated ZnO before and after etching of the sample. The insets (a) and (b) shows the exploded view of the O1s and Zn2p3/2 peaks respectively.

Figure 4. The comparison of high precision scans of Mo3d (a, b), O1s (c, d) and $Zn2p_{3/2}$ (e, f) core levels before and after etching of the sample.

Figure 5. The comparison of high resolution (220,000×) FESEM images of (a) ZnO, (b) 1 wt% (c) 3 wt% and (d) 5 wt% MoO_3 coated ZnO.

Figure 6. The typical TEM images of 5 wt% MoO_3 coated ZnO at various resolutions (a and b). The typical HRTEM images of 5 wt% MoO_3 coated ZnO (c) focusing the interfacial region (d) the measurement of the d-spacing of MoO_3 coating and ZnO. The SAED patterns of the MoO_3 coating and ZnO base are presented in (e) and (f) respectively.

Figure 7. The comparison of (a) decrease in concentration (b) release of Cl^- ions (c) percentage degradation of MCAA whereas the (d) shows the graphical evaluation of rate constant for the degradation of MCAA in sunlight exposure in the presence of bare and MoO_3 coated ZnO powders.

Figure 8. The Mott-Schottky plots of bare and MoO_3 coated ZnO in (a) the dark and (b) under illumination whereas (c) and (d) presents the graphical evaluation of the flat band (V_{fb}) potential under both conditions.

Figure 9. The comparison of IC profiles of TCAA removal over (a) ZnO (b) 1 wt% MoO_3 coated ZnO (c) TiO_2 (degussa P-25) whereas the (d) shows the comparison of TCAA removal over bare, 1 wt% MoO_3 coated ZnO and degussa P-25 powders.

Figure 10. The comparison of the degradation (%) and the graphical evaluation of the rate constant for the degradation of MCAA over 1 wt% MoO_3 coated ZnO with and without dissolved O_2 (a and b). The comparison of IC profiles for the removal of (c) MCAA (d) DCAA over 1 wt% MoO_3 coated ZnO whereas (e) and (f) shows the comparison of photonic efficiencies for the removal of MCAA and DCAA, respectively.

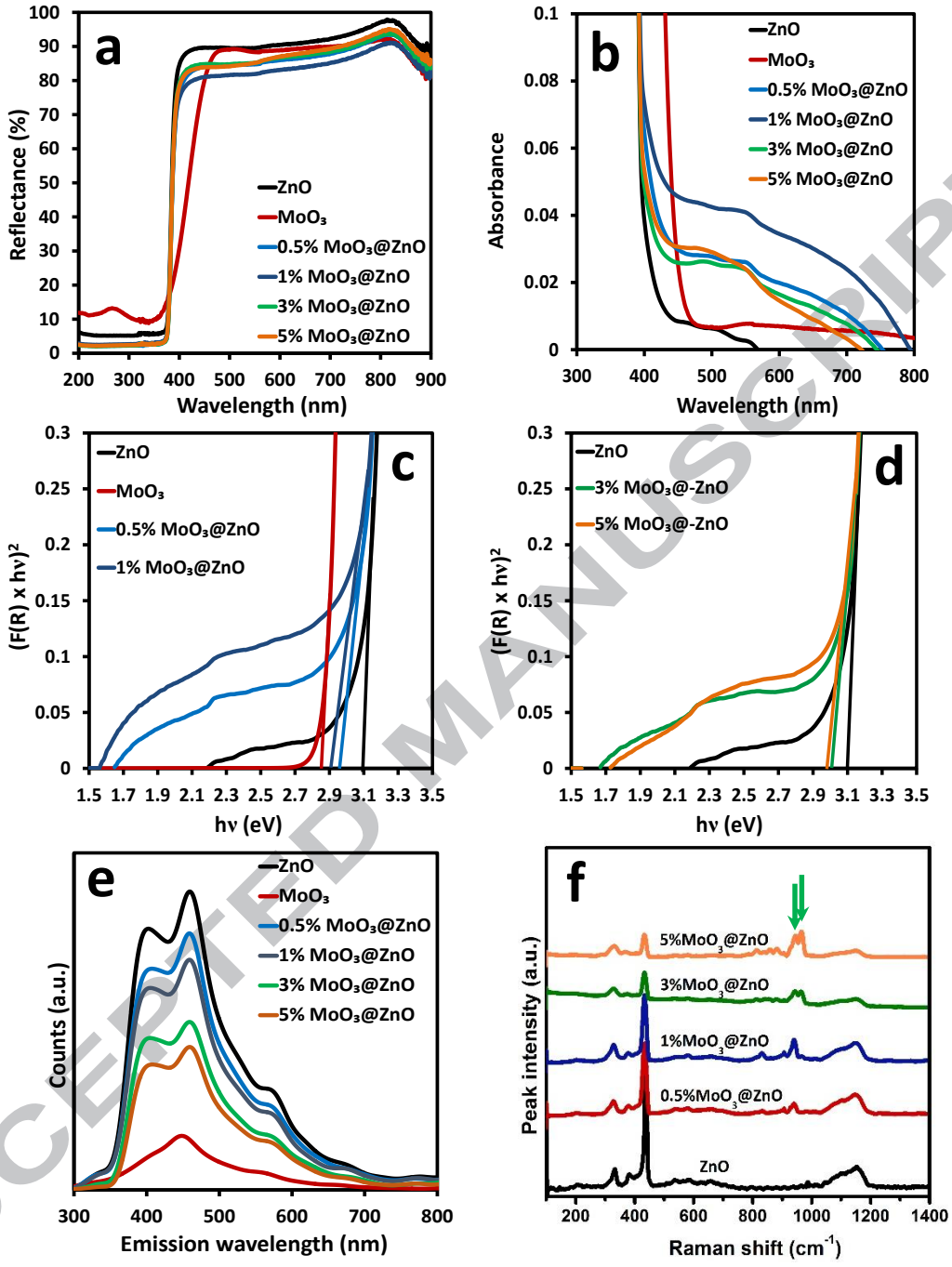

Fig. 1. The comparison of (a) the DR spectra in the range of 200 to 900 nm (b) the solid-state absorption spectra in 300 to 800 nm range. The graphical evaluation of the band edges (c) ZnO, MoO_3, 0.5 and 1 wt% MoO_3 coated ZnO (d) ZnO, 3 and 5 wt% MoO_3 coated ZnO whereas (e) and (f) compares the PL and Raman spectra of bare ZnO and MoO_3 coated ZnO powders respectively.

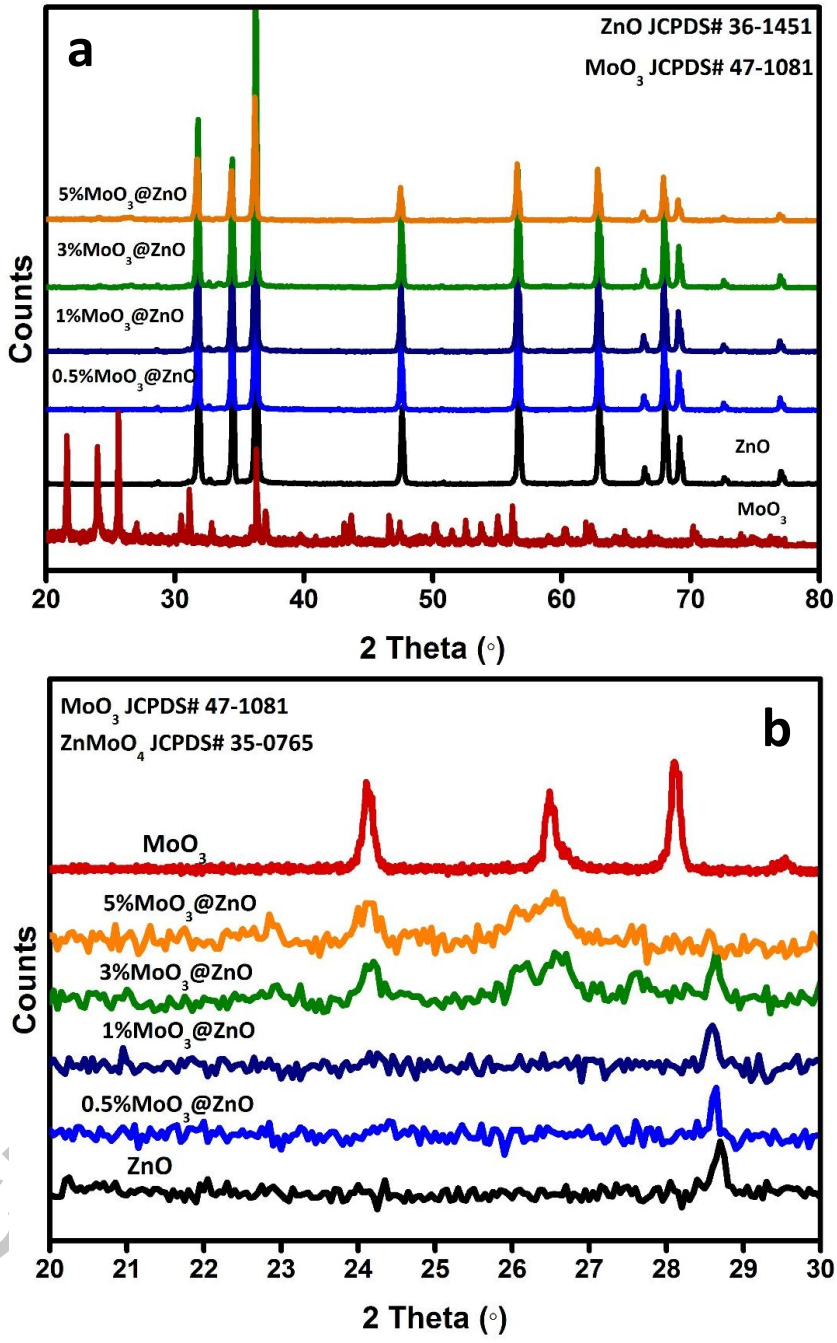

Fig. 2. The comparison of (a) XRD patterns of ZnO, MoO_3, and MoO_3 coated ZnO in the 2θ range of 20º to 80º (b) the exploded view from 2θ = 20° to 2θ = 30° showing the growth of the reflections due to the MoO_3 coating and respective *hkl* indices.

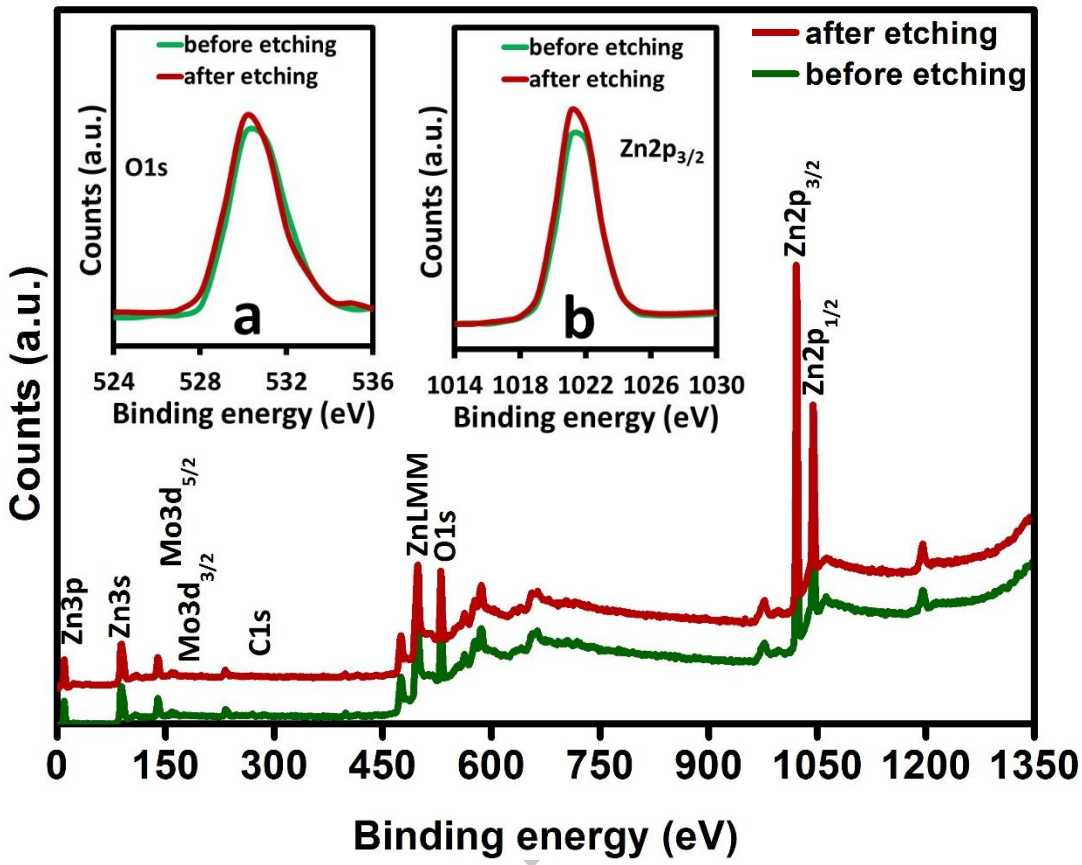

Fig. 3. The comparison of wide angle survey scans of 3 wt% MoO_3 coated ZnO before and after etching of the sample. The insets (a) and (b) shows the exploded view of the O1s and Zn2p3/2 peaks respectively.

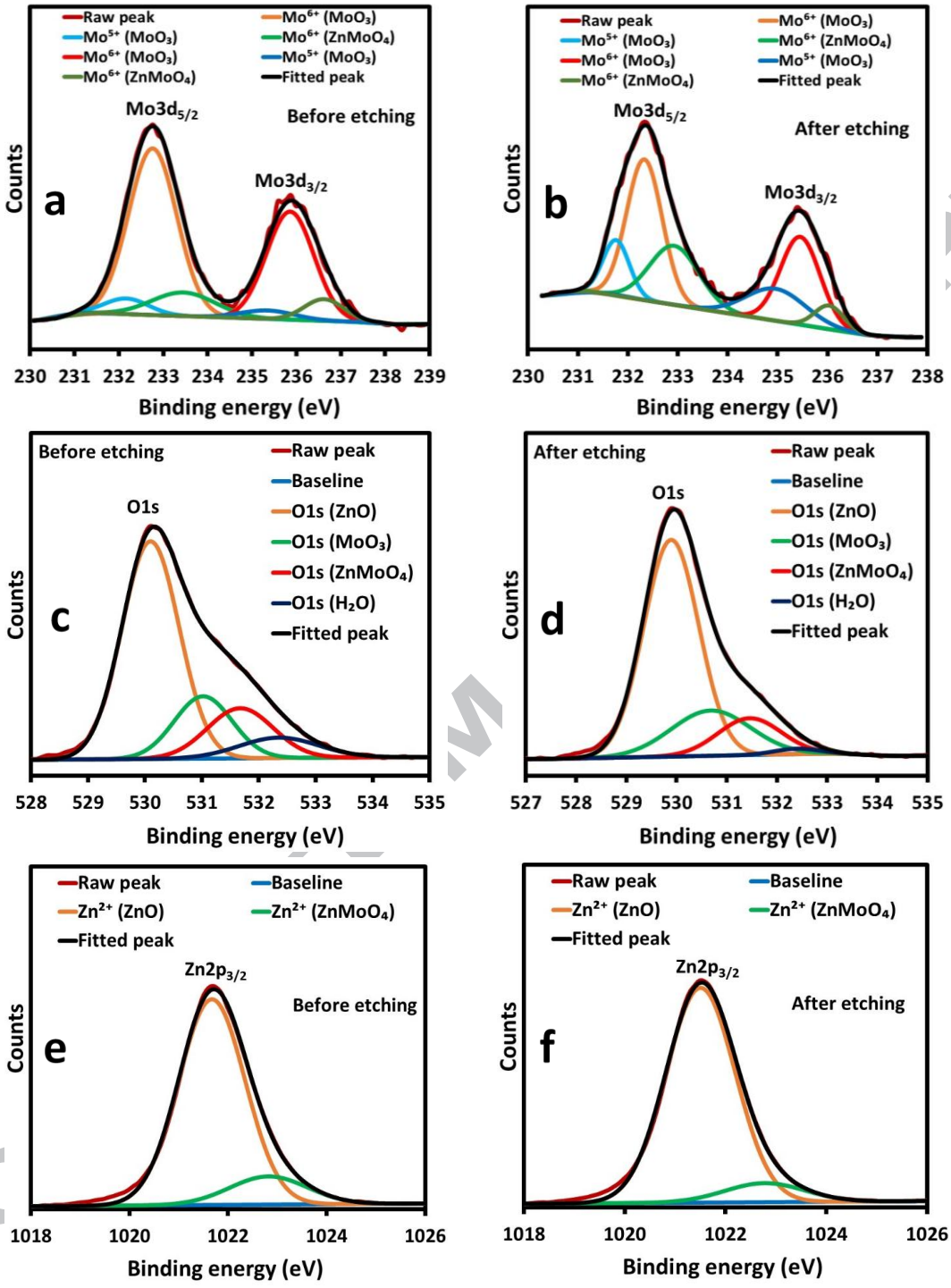

Fig. 4. The comparison of high precision scans of Mo3d (a, b), O1s (c, d) and $Zn2p_{3/2}$ (e, f) core levels before and after etching of the sample.

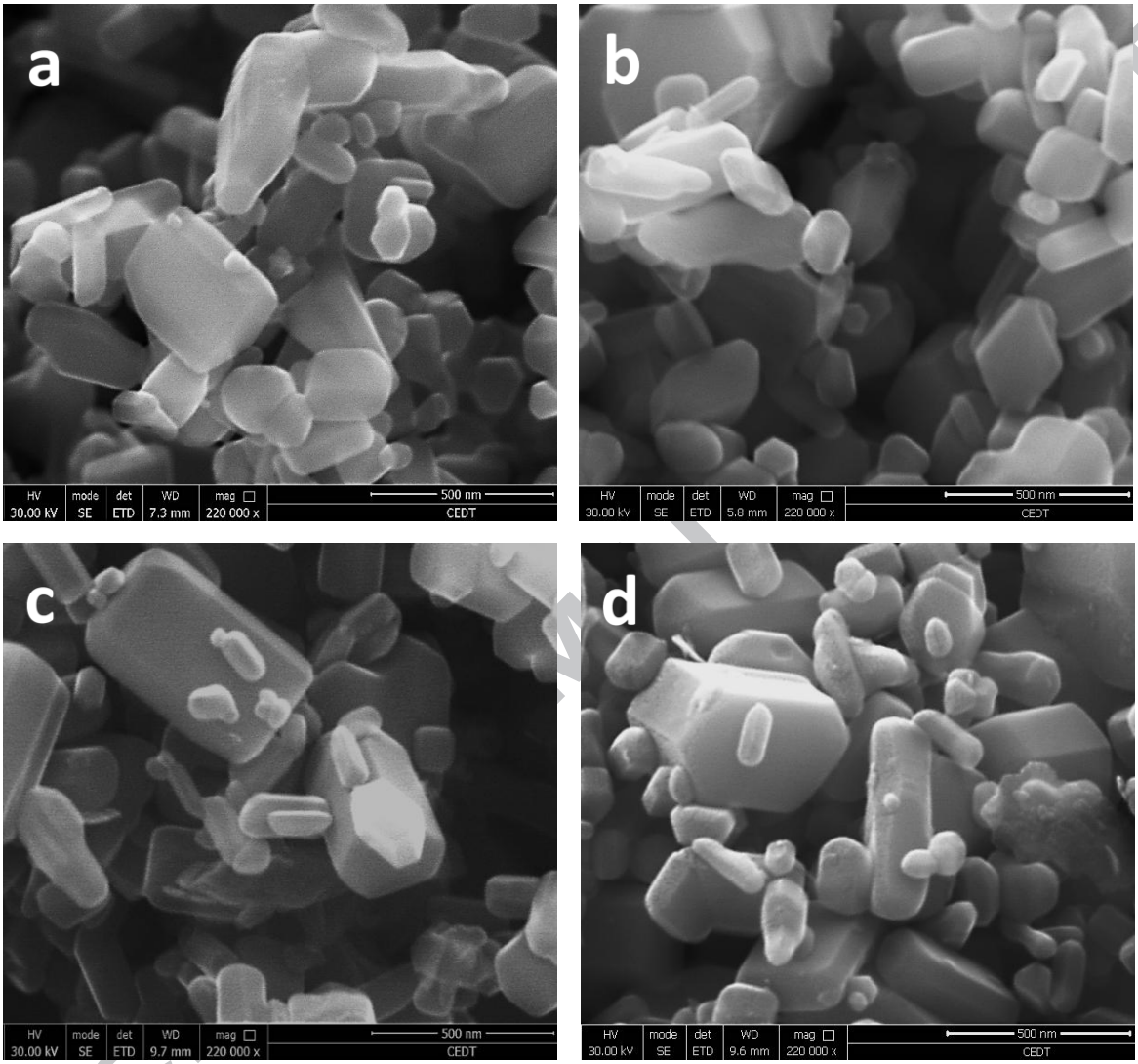

Fig. 5. The comparison of high resolution (220,000×) FESEM images of (a) ZnO, (b) 1 wt% (c) 3 wt% and (d) 5 wt% MoO_3 coated ZnO.

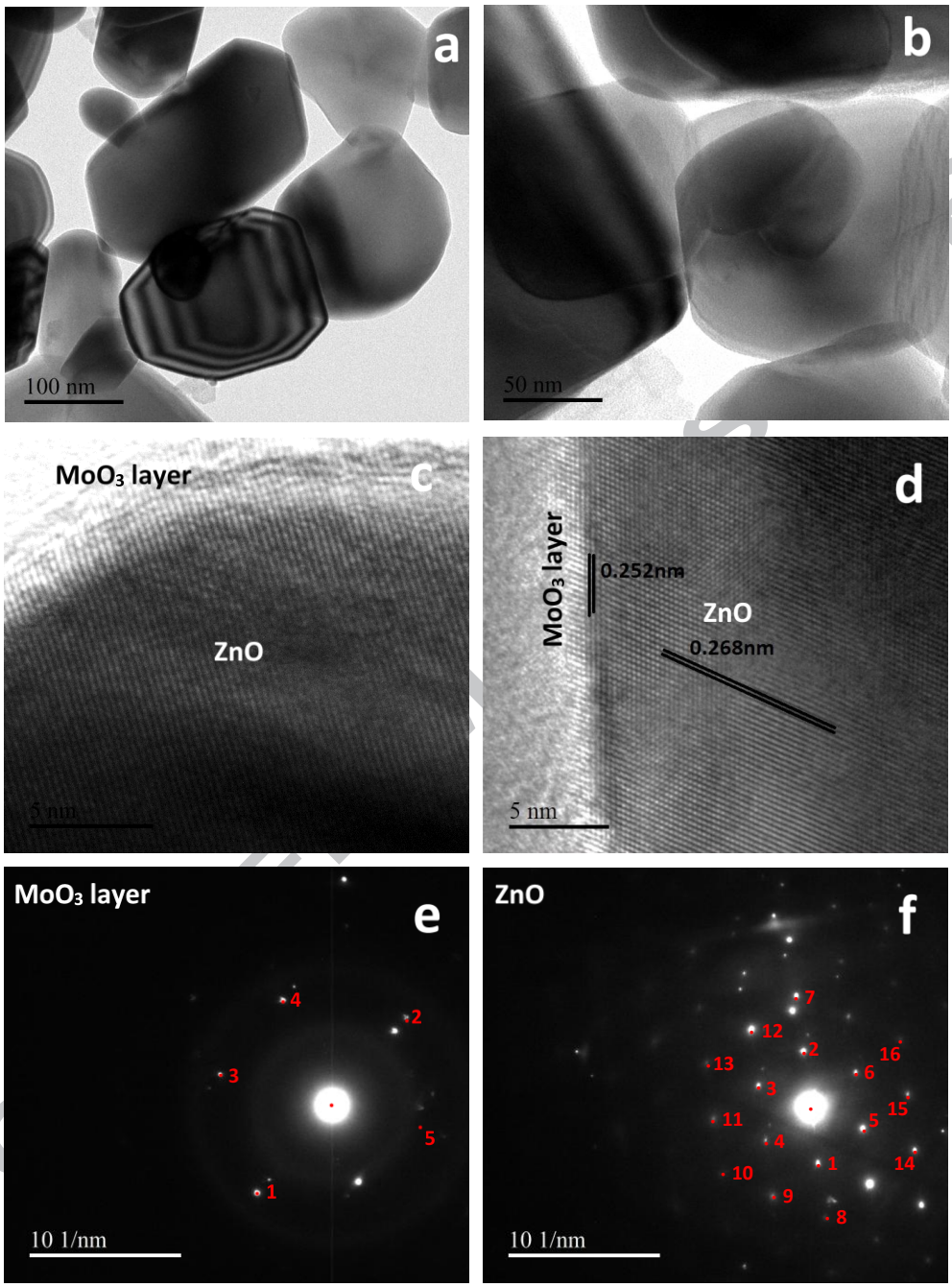

Fig. 6. The typical TEM images of 5 wt% MoO_3 coated ZnO at various resolutions (a and b). The typical HRTEM images of 5 wt% MoO_3 coated ZnO (c) focusing the interfacial region (d) the measurement of the d-spacing of MoO_3 coating and ZnO. The SAED patterns of the MoO_3 coating and ZnO base are presented in (e) and (f) respectively.

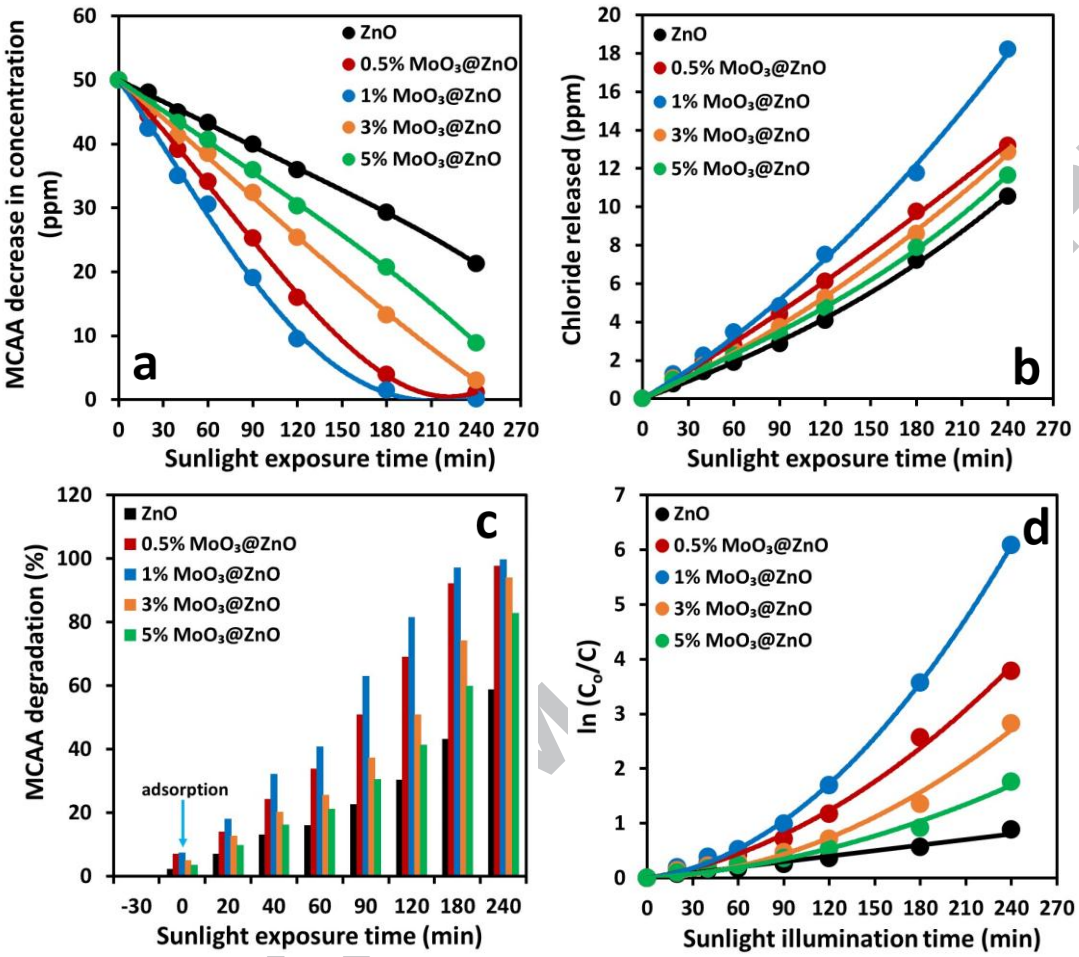

Fig. 7. The comparison of (a) decrease in concentration (b) release of Cl^- ions (c) percentage degradation of MCAA whereas the (d) shows the graphical evaluation of rate constant for the degradation of MCAA in sunlight exposure in the presence of bare and MoO_3 coated ZnO powders.

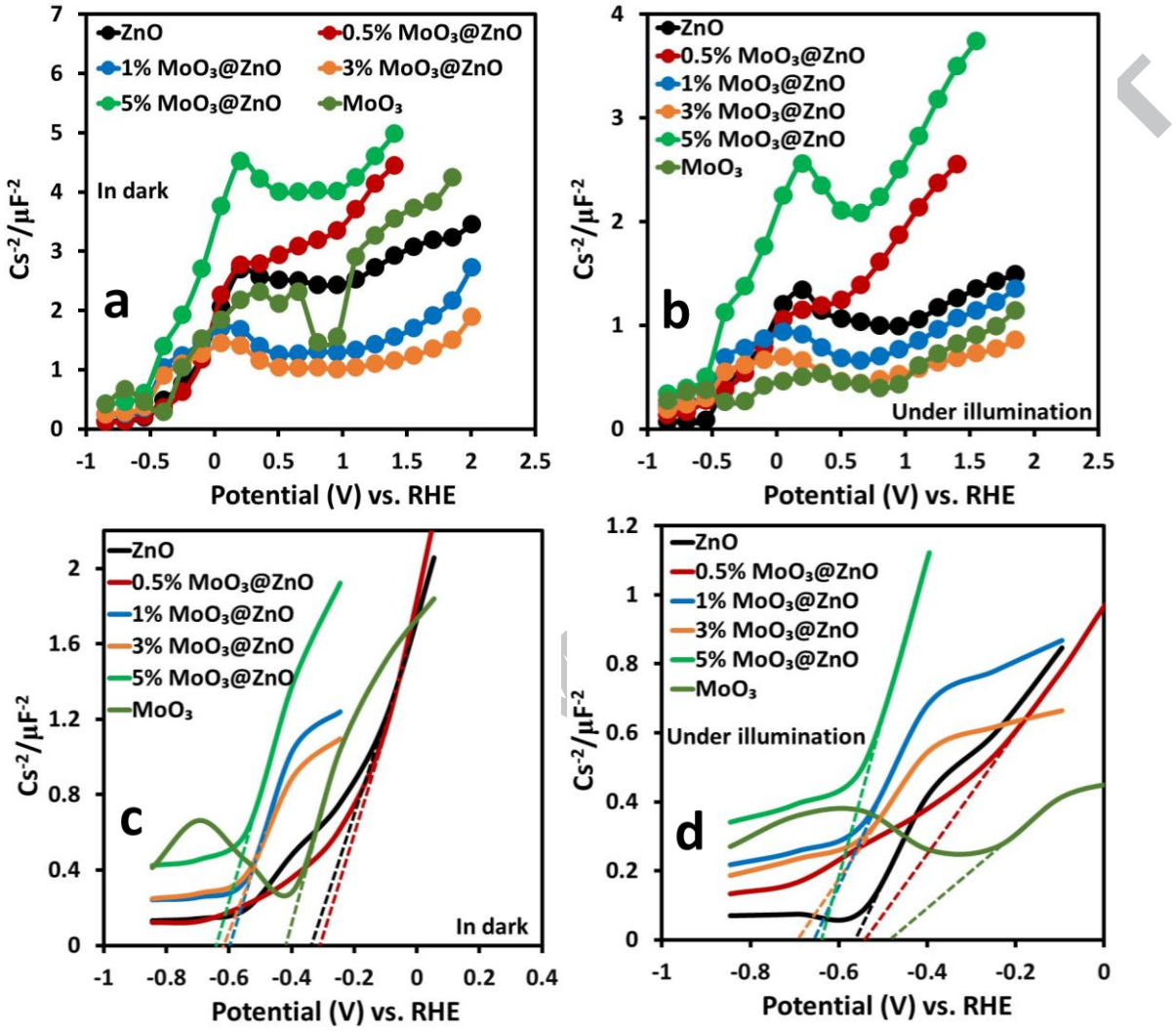

Fig. 8. The Mott-Schottky plots of bare and MoO_3 coated ZnO in (a) the dark and (b) under illumination whereas (c) and (d) presents the graphical evaluation of the flat band (V_{fb}) potential under both conditions.

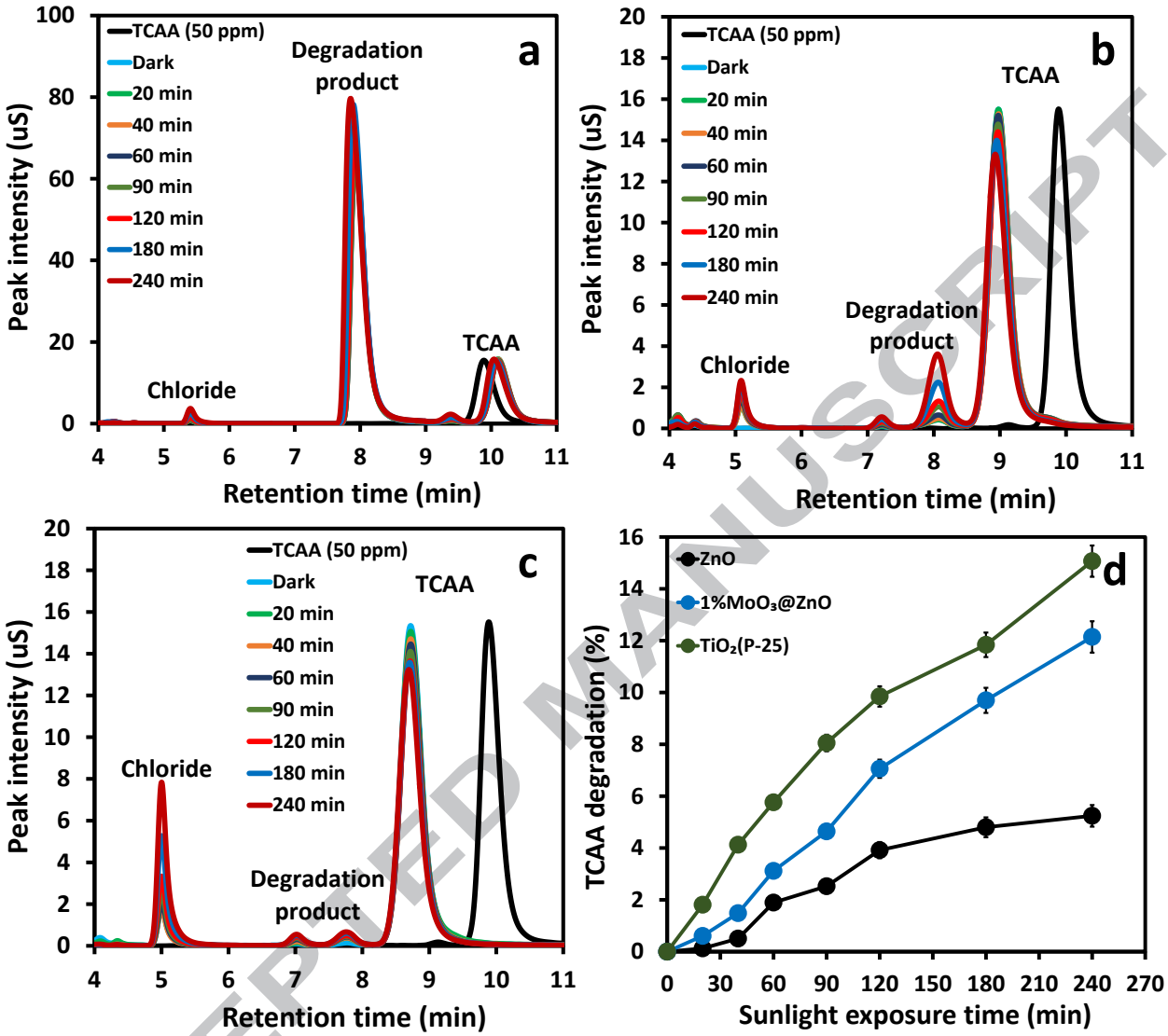

Fig. 9. The comparison of IC profiles of TCAA removal over (a) ZnO (b) 1 wt% MoO_3 coated ZnO (c) TiO_2 (degussa P-25) whereas the (d) shows the comparison of TCAA removal over bare, 1 wt% MoO_3 coated ZnO and degussa P-25 powders.

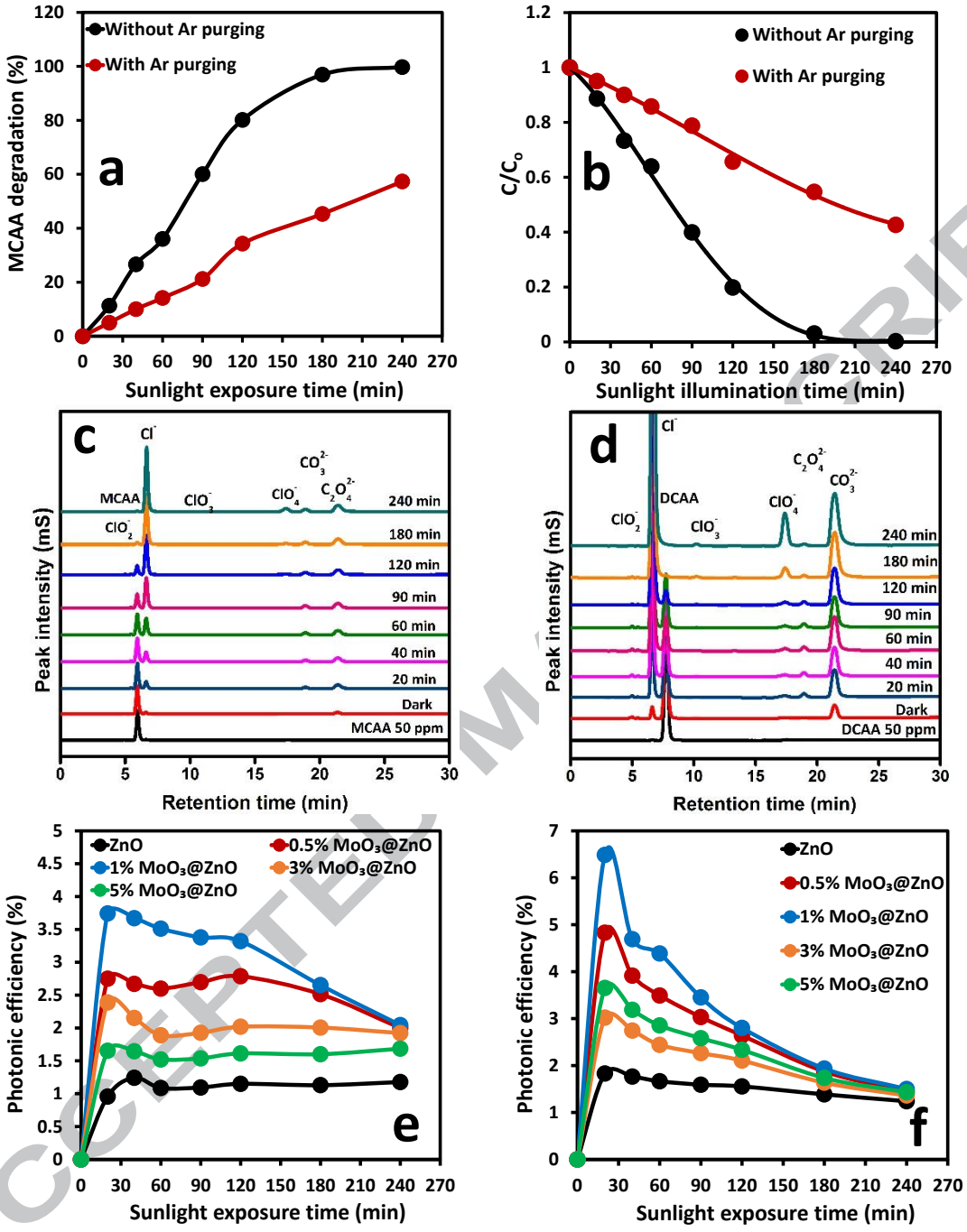

Fig. 10. The comparison of the degradation (%) and the graphical evaluation of the rate constant for the degradation of MCAA over 1 wt% MoO_3 coated ZnO with and without dissolved O_2 (a and b). The comparison of IC profiles for the removal of (c) MCAA (d) DCAA over 1 wt% MoO_3 coated ZnO whereas (e) and (f) shows the comparison of photonic efficiencies for the removal of MCAA and DCAA, respectively.

Graphical Abstract

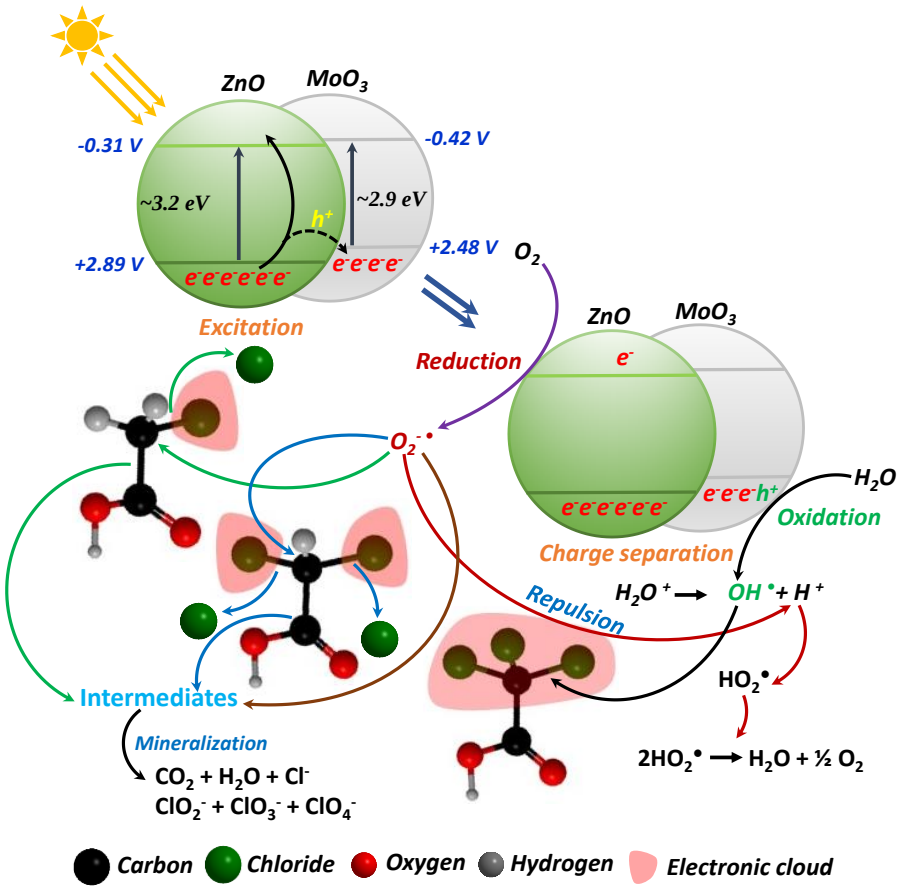

Highlights

- Initially permeate Mo^{6+} ions at the surface of ZnO and finally transformed to MoO_3 by thermal treatment in air.
- The MoO_3 coating protect the surface of ZnO against photocorrosion and excitons recombination.
- The suitability of the band edge positions proposed $O_2^{\bullet -}$ radicals as the majority oxidizers.
- The polarity induced by the Cl groups facilitates the removal of chloroacetic acids derivatives.